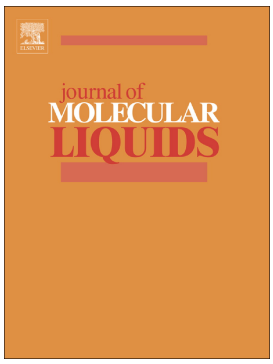

Benzimidazole derivatives as novel inhibitors for the corrosion of mild steel in acidic solution: Experimental and theoretical studies

G.A. Zhang, X.M. Hou, B.S. Hou, H.F. Liu

PII: S0167-7322(18)33908-4
DOI: https://doi.org/10.1016/j.molliq.2019.01.060
Reference: MOLLIQ 10291

To appear in: *Journal of Molecular Liquids*

Received date: 30 July 2018
Revised date: 22 December 2018
Accepted date: 10 January 2019

Please cite this article as: G.A. Zhang, X.M. Hou, B.S. Hou, H.F. Liu , Benzimidazole derivatives as novel inhibitors for the corrosion of mild steel in acidic solution: Experimental and theoretical studies. Molliq (2019), https://doi.org/10.1016/j.molliq.2019.01.060

Benzimidazole derivatives as novel inhibitors for the corrosion of mild steel in acidic solution: experimental and theoretical studies

G. A. Zhang [a,*] X. M. Hou [a] B. S. Hou [a] H. F. Liu[a, b]

[a] *Key Laboratory of Material Chemistry for Energy Conversion and Storage, Ministry of Education, Hubei Key Laboratory of Materials Chemistry and Service Failure, School of Chemistry and Chemical Engineering, Huazhong University of Science and Technology, Wuhan 430074, P.R. China*

[b] *State Key Laboratory of Coal Combustion, Huazhong University of Science and Technology, Wuhan 410074, P.R. China*

Abstract: The inhibition effects of three kinds of benzimidazole derivatives (2-mercaptobenzimidazole (MBI), 2-thiobenzylbenzimidazole (TBBI) and 1-butyl-2-thiobenzylbenzimidazole (BTBBI)) on the corrosion of mild steel in 1 M HCl solution were studied by weight loss and electrochemical measurements, and theoretical calculations. It is found that these compounds act as mixed type inhibitors with predominant cathodic effectiveness and exhibit high inhibition efficiencies with the order: BTBBI > TBBI > MBI. Molecular dynamics simulations reveal that these benzimidazole derivatives adsorb on Fe (1 1 0) surface in flat orientation. The theoretical calculations are in good accordance with the weight loss and electrochemical measurements.

Keywords: Mild steel; Inhibitors; Weight loss measurements; Electrochemical measurements; Theoretical calculations

* Corresponding author; Tel.: +86-27-87559068; Fax: +86-27-87543632
E-mail address: zhangguoan@gmail.com (G.A. Zhang)

1. Introduction

Mild steels are extensively used in industry because of their good mechanical performances and relatively low cost [1-3]. However, their poor corrosion resistances in aggressive environments hinder their practical applications in industrial production. During the oil well acidification and industrial pickling process, severe corrosion of mild steels will occur in the acidic solutions. Adding corrosion inhibitors is an effective method to inhibit the corrosion of mild steels [4-11].

It is suggested [12-15] that the organic compounds containing heteroatoms (O, N, S) possess lone pairs of electrons, which makes them particularly effective as corrosion inhibitors. The adsorptions of these organic compounds via heteroatoms block the active sites and then inhibit the corrosion of metals. The inhibition effects of the inhibitors with different heteroatoms increase in the order of O < N < S. Furthermore, the multiple bonds or aromatic rings in the organic compounds can provide excellent inhibition performance. The inhibition efficiencies of inhibitors vary with their molecular structures and sizes, heteroatoms, adsorptive tendencies, and the surface charges of metals [5, 16-20].

It has been found that many organic compounds are effective on the inhibition of metal corrosion. Unfortunately, most of these organic inhibitors are toxic and their use is restricted due to the environmental protection. It has been demonstrated that benzimidazole and its derivatives have low toxicity and show the good inhibition effects on the corrosion of metals in acidic media [4-6, 16, 21-28]. For benzimidazole molecules, the N atom and aromatic ring are the suitable sites for bonding to metal

surface [21, 29-33]. The inhibition effects of inhibitors on metal corrosion are dependent upon their chemical structures. Consequently, great efforts have been devoted to studying the inhibition performances of the inhibitors with different substituent groups and substituent positions. Zhang et al. [34] evaluated the inhibition performances of five kinds of imidazole inhibitors with different lengths of alkyl chains. They pointed out that the long alkyl chain, with good hydrophobic property, can form a compact hydrophobic film on the metal surface with a high coverage, which could effectively prevent the mild steel corrosion. Moreover, it has been revealed that an inhibitor containing both N and S atoms could promote its adsorption on the metal surface compared with the inhibitor only containing N or S atom [35, 36]. Although the great achievement has been made in the studies about inhibitors, developing a highly effective inhibitor is still a great challenge due to the diversity of organic compounds.

In this work, three kinds of benzimidazole derivatives, i.e., 2-mercaptobenzimidazole (MBI), 2-thiobenzylbenzimidazole (TBBI), 1-butyl-2-thiobenzylbenzimidazole (BTBBI), were used as the inhibitors for mild steel in HCl solution. The inhibition effects of benzimidazole derivatives were evaluated by weight loss and electrochemical measurements. The relationship between the molecular structures and inhibition performances of these three benzimidazole derivatives was also elucidated by quantum chemical calculations. The adsorbed configurations of these three benzimidazole derivative molecules were predicted by molecular dynamics (MD) simulations.

2. Experimental

2.1. Synthesis of inhibitors

In this work, three kinds of benzimidazole derivatives, i.e., 2-mercaptobenzimidazole (MBI), 2-thiobenzylbenzimidazole (TBBI), 1-butyl-2-thiobenzylbenzimidazole (BTBBI), were used as the inhibitors. Scheme 1 displays the molecular structures of these three benzimidazole derivatives. Among them, MBI was purchased from a chemical reagent company. TBBI was synthesized from MBI referring to a previously described experimental procedure [37]. Typically, 50 mL acetone, 0.02 mol MBI and 0.02 mol KOH were added to a round-bottomed flask. The mixture was heated to the reflux temperature under stirring condition. Then 0.02 mol benzyl chloride was added dropwise. After reaction for 3 h, a large amount of distilled water was added, and then colorless acicular crystals of TBBI precipitated. The obtained product was washed with distilled water, and then filtered and dried to obtain colorless pure acicular TBBI.

BTBBI was synthesized from TBBI. Typically, 150 mL tetrahydrofuran (THF), 0.33 mol KOH, and 0.3 mol TBBI were added to a 500 mL round-bottomed flask. The mixture was heated to reflux temperature under stirring condition. Then 0.33 mol 1-bromobutane was added dropwise. After reaction for 15 h, the mixture was filtrated and the filtrate was rotary evaporated. The products were further purified by column chromatography. Then, a bright yellow liquid (BTBBI) was obtained. Scheme 2 shows the synthetic route for TBBI and BTBBI.

The chemical structures of TBBI and BTBBI were analyzed by nuclear magnetic resonance (NMR) spectroscopy (Fig. 1). The NMR data of the synthesized benzimidazole derivatives: (1) TBBI: ^{1}H NMR (400 MHz, DMSO-d_6): δ (ppm) = 4.577 (s, 2H, -SCH_2), 7.125 (m, 2H, Ar-H), 7.247 (t, 1H, Ar-H), 7.310 (t, 2H, Ar-H), 7.371 (m, 1H, Ar-H), 7.451 (d, 2H, Ar-H), 7.549 (m, 1H, Ar-H), 12.600 (s, 1H, NH). (2) BTBBI: ^{1}H NMR (400 MHz, $CDCl_3$): δ (ppm) = 0.906 (t, 3H, $CH_3(CH_2)_3N$-), 1.309 (m, 2H $(CH_3)CH_2(CH_2)_2N$-), 1.704 (m, 2H, $(CH_3CH_2)CH_2(CH_2)N$-), 4.021 (t, 2H, $(CH_3CH_2CH_2)CH_2N$-), 4.624 (s, 2H, CH_2S-), 7.250 (m, 6H, Ar-H), 7.409 (d, 2H, Ar-H), 7.716 (m, 1H, Ar-H).

2.2. Material and solution

In this work, mild steel was used as the material, with a chemical composition (wt. %) of 0.02% C, 0.3% Mn, 0.017% P, 0.007% S, 0.30% Si, 0.072% Al, and bal. Fe. The sizes of the specimens for weight loss and electrochemical measurements were 50 mm × 10 mm × 3 mm, 10 mm × 10 mm × 3 mm, respectively. For electrochemical measurements, the specimens were embedded into epoxy resin with an exposed area of 1 cm^2. Before testing, the specimens surface were abraded with 800 grit SiC paper. The test solution was 1 M HCl solution, which was prepared with reagent grade HCl (37%) and distilled water.

2.3. Weight loss measurements

The corrosion rate of mild steel in the solution without or with inhibitors was measured by weight loss method. Three parallel specimens were immersed into the solution for 24 h for each condition. After immersion, the specimens were removed,

and the average weight loss was measured to calculate the average weight loss corrosion rate. Then, the inhibition efficiencies (η_w%) of inhibitors were calculated:

$$\eta_w(\%) = \frac{V_0 - V}{V_0} \times 100\% \quad (1)$$

where V_0 and V were the weight loss corrosion rates without and with inhibitors, respectively.

2.4. Electrochemical measurements

For electrochemical measurements, a conventional three-electrode cell was used, with the steel specimen as working electrode (WE), a platinum plate as counter electrode (CE) and a saturated calomel electrode (SCE) as reference electrode (RE). After the WE was immersed in the solution for 1 h and a steady potential reached, electrochemical impedance spectroscopy (EIS) was measured at open circuit potential (OCP) with a amplitude of 5 mV and the frequency from 100,000 to 0.01 Hz. The inhibition efficiencies (η_{EIS}%) of inhibitors were determined by EIS measurements:

$$\eta_{EIS}\% = \frac{R_{ct} - R_{ct}^0}{R_{ct}} \times 100 \quad (2)$$

where R_{ct}^0 and R_{ct} were the charge transfer resistances without and with inhibitors, respectively.

Polarization curves measurements were conducted from -0.2 V to 0.2 V vs. OCP with a sweep rate of 0.5 mV/s. The inhibition efficiencies (η_p %) of inhibitors were also calculated according to the polarization curves:

$$\eta_P\% = \frac{i_{corr}^0 - i_{corr}}{i_{corr}^0} \times 100 \quad (3)$$

where i^0_{corr} and i_{corr} are the corrosion current densities in the solutions without and

with inhibitors, respectively.

2.5. Surface characterization of specimens after corrosion

After being immersed in the solution without or with inhibitors, the specimens were removed from the solution, and cleaned with deionized water. Then, the surface morphologies of the corroded specimens were observed and captured by scanning electron microscope (SEM).

2.6. Quantum chemical calculations

Quantum chemical calculations were conducted with Materials Studio software based on density function theory (DFT). Geometrical optimizations were performed with the generalized gradient approximation (GGA) functional of Becke exchange plus Lee–Yang–Parr correlation (BLYP) method with a double numerical plus polarization (DNP) basis set without any symmetry and spin constraints. In the calculations, solvent effects were considered with water as the solvent. Furthermore, frequency analysis was performed to make sure that there was no imaginary frequency and the obtained structure had the minimum potential energy. The convergence criteria for energy, maximum force, maximum displacement, self-consistent field (SCF) and k-point set were 1.0×10^{-5} Ha, 2.0×10^{-3} Ha/Å, 5.0×10^{-3} Å, 1.0×10^{-6} and 1×1×1, respectively.

2.7. Molecular dynamics simulations

The adsorption process of three kinds of benzimidazole derivative inhibitors on Fe surface was studied by molecular dynamics (MD) simulations. First, 11 layers Fe (1 1 0) surface were cleaved from bcc Fe crystal, and then enlarged to a (13 × 13) supercell. The size of supercell was 3.2 nm × 3.2 nm × 2.0 nm. Then the second layer containing 8 inhibitor molecules and 1000 H_2O molecules in aqueous solution (density 0.997 g/cm^3) was built above the Fe (1 1 0) surface. Above the solution layer, a vacuum slab (a thickness of 20 Å) was built. All the Fe atoms were fixed, and all the inhibitor and H_2O molecules could move freely.

Dynamics simulations were conducted with NVT constant canonical ensemble at 303.15 K. The temperature control method was Berendsen thermostat. The total simulation time was 500 ps with the time step of 1.0 fs.

The average adsorption energy (E_{ads}) of one inhibitor molecule on Fe (1 1 0) surface was calculated:

$$E_{ads} = (E_{inhibitor + surface} - (E_{inhibitor} + E_{surface}))/8 \quad (4)$$

where $E_{inhibitor + surface}$ is the total energy of the Fe (1 1 0) surface together with the 8 adsorbed inhibitor molecules; $E_{inhibitor}$ is the total energy of the 8 free inhibitor molecules; $E_{surface}$ is the energy of Fe (1 1 0) surface.

3. Results and discussion

3.1. Weight loss measurements

Fig. 2 shows the weight loss corrosion rate of mild steel in 1 M HCl solution without or with different concentrations of three kinds of benzimidazole derivative

inhibitors at 30 ^{o}C for 24 h. The corresponding inhibition efficiencies of these three inhibitors are also shown in Fig. 2. It is seen that the corrosion rate of mild steel decreases significantly in the solutions with inhibitors. Furthermore, the corrosion rate decreases with the increasing inhibitor concentration. The inhibition efficiencies of these three kinds of benzimidazole derivatives follow the order: BTBBI > TBBI > MBI. Particularly, the inhibition efficiency of BTBBI reaches 92.75% even in a low concentration of 10 mg/L, and increases to 98.88% with a concentration of 100 mg/L. Therefore, the introduction of benzyl and alkyl chain to 2-mercaptobenzimidazole significantly promotes the inhibition performance for the corrosion of mild steel in acidic solution.

3.2. Electrochemical impedance measurements

Fig. 3 shows the EIS of mild steel in 1 M HCl solution without or with different concentrations of benzimidazole derivatives inhibitors at 30 ^{o}C for 1 h. The Nyquist plots in the solutions without or with inhibitors are similar, i.e., only a single capacitive loop corresponding to the charge transfer resistance and double layer capacitance at the electrode/solution interface during the corrosion process [38]. The similar capacitive loops may indicate that the electrode reactions are controlled by the charge transfer process in the absence or presence of inhibitors [39]. However, the capacitive loop enlarges obviously in the inhibited solution, indicating the great inhibition effect of inhibitors. The impedance increases with inhibitor concentration because of the increasing surface coverage of inhibitor molecules. In the Bode plots,

only one phase angle peak is observed, suggesting one time constant. The frequency range of the maximum phase angle becomes larger in the presence of inhibitors, which suggests the effective adsorption of inhibitors on the mild steel surface [40]. To determine the thermodynamic parameters of the adsorption of inhibitor, the EIS of mild steel in 1 M HCl solution without or with different concentrations of BTBBI at different temperatures for 1 h were also measured, as shown in Fig. 4. It is seen that the Nyquist plots are also characterized by a single capacitive loop, and the impedance decreases with the increasing temperature in the both blank and inhibited solutions.

To obtain the electrochemical parameters, the EIS data were fitted with an equivalent circuit shown in Fig. 5. Table 1 and Table 2 list the corresponding electrochemical parameters. In the equivalent circuit, R_s is the solution resistance; Q_{dl} is the constant phase element (CPE) representing the double layer capacitance; R_{ct} is the charge transfer resistance. The Nyquist plots show a depressed capacitive loop because of the inhomogeneous electrode surface after corrosion [41, 42]. Accordingly, CPE was the used to represent the double layer capacitance (C_{dl}). The value of C_{dl} can be determined from CPE [43, 44]:

$$C_{dl} = Y_0 (2\pi f_{max})^{n-1} \quad (5)$$

where Y_0, n is the magnitude and phase shift constant of CPE, f_{max} is the frequency corresponding to the maximum imaginary value.

It is seen from Table 1 and Table 2 that the R_{ct} increases and the C_{dl} decreases with the increasing inhibitor concentration. The decrease in C_{dl} may be due to the

decreasing dielectric constant and/or the increasing electrical double layer thickness [44]. The increase in R_{ct} suggests an increase in the adsorbed inhibitor molecules. Furthermore, the value of R_{ct} in the inhibited solution increases in the order: MBI < TBBI < BTBBI, i.e., the inhibition efficiency increases in the order: MBI < TBBI < BTBBI. With the increase of temperature, the value of R_{ct} in the solution with BTBBI decreases.

3.3. Polarization curves measurements

Fig. 6 shows the polarization curves of mild steel in 1 M HCl solution without or with various concentrations of inhibitors at 30 ^{o}C for 1 h. Both the anodic and cathodic current densities decrease after adding inhibitors, which suggests that the presence of inhibitors not only inhibits the anodic dissolution of steel but also suppresses the cathodic hydrogen evolution [14, 45]. Furthermore, the inhibition of cathodic reaction is more significant than that of anodic reaction, which leads to a negative shift of corrosion potential (E_{corr}) after adding inhibitors. The negative shift of E_{corr} is less than 85 mV, which indicates that these benzimidazole derivatives act as mixed-type inhibitors with predominant cathodic effectiveness [2, 46, 47]. Fig. 7 shows the polarization curves of mild steel in 1 M HCl solution without or with different concentrations of BTBBI at different temperatures for 1 h. Both the anodic and cathodic current densities are reduced in the presence of BTBBI inhibitor at various temperatures.

The values of corresponding electrochemical parameters, including corrosion

potential (E_{corr}), corrosion current density (i_{corr}), anodic and cathodic Tafel slopes (b_a, b_c), which were determined by extrapolation, are presented in Table 3 and Table 4. It is clear that the corrosion current densities after adding inhibitors are much less than those without inhibitors. Furthermore, the corrosion current densities in the solutions with BTBBI are much less than those in the solutions with TBBI or MBI, indicating the higher inhibition efficiency of BTBBI. Additionally, the corrosion current densities in the solutions without or with BTBBI increase with the increase of temperature.

3.4. Adsorption isotherms

To determine the adsorption behavior of benzimidazole derivatives inhibitors, the corresponding absorption isotherms were evaluated. It is found that the absorption behavior of these three benzimidazole derivatives follows the Langmuir adsorption isotherm [47, 48]:

$$\frac{C_{inh}}{\theta} = \frac{1}{K_{ads}} + C_{inh} \quad (6)$$

where C_{inh} is the inhibitor concentration, mol/L; θ is the surface coverage of inhibitors, which is equal to the inhibition efficiency determined by EIS ($\theta = \eta_{EIS}$); K_{ads} is the adsorption equilibrium constant, which is obtained by the reciprocal of the intercept of C/θ axis. The plots of C/θ vs. C and the corresponding linear fitted straight lines for MBI, TBBI, and BTBBI at 30 ^{o}C are shown in Fig. 8. It can be seen that all these straight lines have the correlation coefficient more than 0.99, which confirms that the adsorption of these inhibitors follows the Langmuir adsorption isotherm. After the

value of K_{ads} is determined by the adsorption isotherm, the standard free energy of adsorption (ΔG^{o}_{ads}) can be calculated [48]:

$$\Delta G^{o}_{ads} = -RT \ln(55.5 K_{ads}) \quad (7)$$

where R is the gas constant (8.314 J/(mol K)), and T is the absolute temperature (K). Table 5 lists the values of K_{ads} and ΔG^{o}_{ads} for MBI, TBBI and BTBBI. The large negative value of ΔG^{o}_{ads} indicates the spontaneous adsorption of inhibitors by a strong interaction with the steel surface. It is acknowledged [13, 49] that, when ΔG^{o}_{ads} > -20 kJ/mol, inhibitors can adsorb on metal surface by electrostatic interaction (physisorption). When ΔG^{o}_{ads} < -40 kJ/mol, coordinate bonds (chemisorption) are formed by charge sharing or transferring from inhibitors to metal surface. When -40 kJ/mol < ΔG^{o}_{ads} < -20 kJ/mol, the adsorption of inhibitors involves both physisorption and chemisorption [50]. It is clear from Table 5 that the adsorption of MBI and TBBI is a mixed type including both physisorption and chemisorption, while the absorption of BTBBI is typical chemisorption. Generally, the higher values of K_{ads} and ΔG^{o}_{ads}, the higher adsorption ability and then higher inhibitive effect of inhibitor. Therefore, there is higher adsorption ability and inhibitive effect of BTBBI with higher values of K_{ads} and ΔG^{o}_{ads}.

To determine the enthalpy (ΔH^{o}_{ads}) and entropy (ΔS^{o}_{ads}) of the adsorption of inhibitor, EIS and polarization curves measurements for mild steel in 1 M HCl solution without or with different concentrations of BTBBI inhibitor were performed at different temperatures for 1 h. The corresponding plots of C/θ vs. C and the linear fitted straight lines are shown in Fig. 9. After the values of K_{ads} at different

temperatures were determined by the adsorption isotherms, the thermodynamic parameters, ΔH_{ads}^{o} and ΔS_{ads}^{o}, could be calculated according to following equation [51]:

$$\ln K_{ads} = -\frac{\Delta H_{ads}^{o}}{RT} + \frac{\Delta S_{ads}^{o}}{R} - \ln(55.5) \quad (8)$$

Fig. 10 shows the linear relationship between lnK_{ads} and 1/T for mild steel in 1 M HCl solution with different concentrations of BTBBI inhibitor. The values of ΔH_{ads}^{o} and ΔS_{ads}^{o} of the adsorption of BTBBI inhibitor were determined by the slope and intercept of the lnK_{ads} ~1/T plots. Table 6 lists the standard free energy (ΔG_{ads}^{o}), enthalpy (ΔH_{ads}^{o}), and entropy (ΔS_{ads}^{o}) of the adsorption of BTBBI inhibitor at different temperatures. It is seen that the value of ΔH_{ads}^{o} is negative, indicating an exothermic process of the adsorption of BTBBI on the mild steel surface. The positive sign of ΔS_{ads}^{o} indicates that the adsorption process of BTBBI accompanies an increase in entropy, which serves as the driving force for the adsorption of inhibitor on the mild steel surface.

3.5. Corrosion kinetic analysis

To determine the kinetic parameters of the corrosion process of mild steel in the solutions without or with inhibitors, polarization curves measurements were conducted at various temperatures. Then the activation energy (E_a), enthalpy (ΔH_a) and entropy (ΔS_a) of activation were determined by following equations [52]:

$$i_{corr} = A\exp(-\frac{E_a}{RT}) \quad (9)$$

$$\ln\frac{i_{corr}}{T} = \ln\frac{R}{Nh} + \frac{\Delta S_a}{R} - \frac{\Delta H_a}{RT} \quad (10)$$

where A is the pre-exponential constant. h is the Plank's constant and N is the Avogadro's number.

Fig. 11 and Fig. 12 show the Arrhenius plots of $\ln i_{corr}$ vs. $1/T$ and the transition state plots of $\ln(i_{corr}/T)$ vs. $1/T$ in the solutions without or with 50 mg/L MBI, TBBI and BTBBI. Based on the equations (9) and (10), the values of E_a, ΔH_a and ΔS_a can be obtained by the slopes and intercepts of the straight lines, and their values are presented in Table 7. It is seen that the value of E_a in the solution without inhibitor is 51.73 kJ/mol, while in the solutions with MBI or TBBI, the values of E_a are 56.20 and 54.12 kJ/mol, respectively, which are a little higher than that in the blank solution. The E_a of BTBBI is 27.27 kJ/mol, which is much lower than that in the solution without inhibitor. The low E_a of BTBBI may be ascribed to the formation of strong chemisorption between the BTBBI molecules and steel [36]. The value of ΔH_a is relatively close and follow the same pattern as the value of E_a, which is in line with the concept of transition-state theory. Furthermore, the value of ΔH_a is positive, indicating an endothermic process of the mild steel dissolution. This has also been reported to be indicative of the retarded dissolution of metal in the solution with inhibitor [53]. The negative value of ΔS_a suggests that the activated complex is associative rather than dissociative in the rate determining step, i.e., transition from reactants to activated complex is accompanied by increase in orderliness [54].

3.6. SEM surface morphology after corrosion

Fig. 13 shows the SEM surface morphologies of the specimens after exposed in 1 M HCl solution without or with 50 mg/L MBI, TBBI, BTBBI inhibitors at 30 ^{o}C for 24 h. It is seen that severe corrosion occurs on the specimens in the solution without inhibitor. A large amount of corrosion products are observed on the whole specimen surface. After adding inhibitors, the specimen surface is relatively smooth and the scratches produced during the abrasion pretreatment process are still observed. This indicates that the adsorption of inhibitor to some extent prevents the contact between the steel and aggressive species. Furthermore, the corrosion of the specimens in the solution with BTBBI is slighter than those in the solutions with TBBI or MBI, suggesting a higher inhibition performance of BTBBI.

3.7. Stability of the inhibition effect

To determine the long-term inhibition effects of inhibitors, the specimens were immersed in the solution containing 50 mg/L each inhibitor for 72 h, and the time dependence of the inhibitor efficiency of each inhibitor was determined by EIS measurements, as shown in Fig. 14. The inhibition efficiency of MBI drops quickly with immersion time and loses its inhibition effect after 24 h. For TBBI, the decrease in inhibition efficiency is slow and the inhibition efficiency drops to 90% after 72 h. However, BTBBI always shows an excellent inhibition performance with an inhibition efficiency more than 97.4% during the whole immersion time. This indicates that benzene ring and alkyl chain contribute to strong absorption of BTBBI on the specimen surface with long-term stable inhibition effect.

3.8. Quantum chemical calculations

It has been demonstrated that quantum chemical calculation is the useful way to theoretically elucidate the correlation between the inhibitor molecule structure and its inhibition mechanism at a molecular level. According to the frontier molecular orbitals (FMO) theory, the highest occupied molecular orbital (HOMO) is associated with the ability of inhibitor to donate electrons, while the lowest unoccupied molecular orbital (LUMO) is related to the ability of inhibitor to accept electrons [55]. The energy band gap ($\Delta E = E_{LUMO} - E_{HOMO}$) indicates the activity of inhibitor to adsorb on metal surface.

Fig. 15 shows that the optimized molecular structures of the three benzimidazole derivatives (MBI, TBBI, BTBBI). It is seen that MBI presents a rigid planar structure of the benzimidazole segment and sulfydryl group, while the benzene ring and alkyl chain in TBBI and BTBBI are not in the plane with benzimidazole ring. Fig. 16 shows the HOMO and LUMO distributions of these three benzimidazole derivatives. The electron densities of HOMO for these three benzimidazole derivatives mostly locate at the benzimidazole ring and sulfydryl group. These Benzimidazole derivatives could donate electrons to the steel to form coordinate bonds at these positions. For MBI, the electron densities of LUMO also locate at the benzimidazole ring and sulfydryl group, while for TBBI and BTBBI, the electron densities of LUMO locate at the benzene ring and sulfydryl group. These positions could be acceptor of electrons from steel to form feedback bonds.

Additionally, the electronegativity (χ) and global hardness (γ) of inhibitor molecules can be calculated with E_{HOMO} and E_{LUMO} [24]:

$$\chi = -\frac{E_{HOMO} + E_{LUMO}}{2} \quad (9)$$

$$\gamma = \frac{E_{LUMO} - E_{HOMO}}{2} \quad (10)$$

Then the fraction of electron transferred (ΔN) can be determined with the electronegativities and global hardnesses of inhibitor molecules (χ_{inh}, γ_{inh}) and Fe atom (χ_{Fe}, γ_{Fe}) [56]:

$$\Delta N = \frac{\chi_{Fe} - \chi_{inh}}{2(\gamma_{Fe} + \gamma_{inh})} \quad (11)$$

The theoretical values of χ_{Fe} and γ_{Fe} are 7 eV and 0 eV, respectively [57]. The parameter of ΔN reflects the inhibition performance from electrons donation. If ΔN < 3.6, the chemisorption and inhibition efficiency increase with the electron-donating ability [58].

Table 8 lists the quantum parameters of these three benzimidazole derivatives. It is suggested that the values of $E_{HOMO,}$ E_{LUMO} and ΔE are associated with the inhibition efficiencies of inhibitors. A higher E_{HOMO} and lower ΔE corresponds to a stronger chemisorption of inhibitor molecules, and then higher inhibition efficiency. From Table 8, the ΔE of these three inhibitors follows the order: MBI > TBBI > BTBBI, while the ΔN of these three inhibitors is in the order of MBI < TBBI < BTBBI. Therefore, the inhibition performances of these three benzimidazole derivatives follow the order: MBI < TBBI < BTBBI.

To elucidate the local reactive sites in inhibitor molecules, Fukui indices (f_k^+ , f_k^-)

were determined. It is well known that the atoms with higher values of f_k^+ or f_k^- have higher abilities to accept or donate electrons, i.e., susceptible to be attacked by a nucleophilic reagent or an electrophilic reagent, respectively. Table 9 lists the Fukui indices (mulliken) of the atoms of inhibitors. For MBI, the high value of f_k^+ is present at C2, C5, C8, and S10, indicating the high susceptibility of nucleophilic attack at these sites, while high value of f_k^- is present at C1, C3, N7, and S10, i.e., these sites are susceptible to electrophilic attack. For TBBI and BTBBI, the high value of f_k^+ is present at the benzene ring and sulfydryl group, while the high value of f_k^- is present at the benzimidazole ring and sulfydryl group. Therefore, the benzene ring and sulfydryl group are susceptible to nucleophilic attack, and the benzimidazole ring and sulfydryl group are susceptible to electrophilic attack.

3.9. Molecular dynamics (MD) simulations

MD simulations were conducted to study the adsorption behavior of the benzimidazole derivatives on Fe (1 1 0) surface. As shown in Fig. 17, both MBI and TBBI molecules adsorb on the Fe surface with a flat orientation. The adsorption of MBI molecules is through forming coordinate bonds between the benzimidazole ring and sulfydryl group and the Fe surface. For TBBI, apart from the adsorptions of benzimidazole ring and sulfydryl group, benzene ring also adsorb on the Fe surface by forming feedback bonds. During the adsorption, a twirling of benzene ring occurs so that benzimidazole ring, sulfydryl group, and benzene ring adsorb on the Fe surface in a flat orientation. The adsorption of BTBBI on Fe surface is also by the adsorptions of

benzimidazole ring, sulfydryl group, and benzene ring in a flat orientation. Meanwhile, the alkyl chain arranges far from the Fe surface to form a hydrophobic layer. The calculated adsorption energies (E_{ads}) of these three benzimidazole derivatives are listed in Table 10. The adsorption energies (E_{ads}) of these three benzimidazole derivative inhibitors are in the order: BTBBI < TBBI < MBI. Generally, a more negative adsorption energy means a higher inhibition efficiency of inhibitor. Therefore, it is expected that the inhibition efficiencies of these three benzimidazole derivatives follow the order: BTBBI > TBBI > MBI. The MD simulations are consistent with the weight loss and electrochemical measurements.

3.10. Inhibition mechanism of benzimidazole derivative inhibitors

The adsorption behavior of inhibitor molecules is dependent upon their physicochemical properties (e.g. functional groups, electron density) and the charge of metal surface. Based on the experimental measurement results and theoretical calculations, a possible inhibition mechanism of these three benzimidazole derivatives on Fe surface is elucidated in Fig.18. A lot of research have indicated that the mild steel surface is positively charged in HCl solution, i.e., there are excess positive charges on the steel surface [14, 31, 59, 60]. The positively charged specimen surface favors the adsorption of Cl^- to create a negative charge surface, which facilitates the adsorption of the cations in the solution. These benzimidazole derivatives molecules may be protonated in the solution because of the unshared electron pair of the N and S atoms. The protonated molecules could adsorb on specimen surface via electrostatic

interaction, i.e., physisorption (Fig. 18(a)). Meanwhile, further adsorption of these inhibitor molecules could be realized by forming covalent bonds (chemisorption), as shown in Fig. 18(b). Quantum chemical calculations and MD simulations demonstrate that both the HOMO and LUMO of MBI molecules locate at the benzimidazole ring and sulfydryl group, where the MBI molecules could adsorb on the specimen surface in a flat orientation by forming coordinate bonds and/or feedback bonds. The absorption isotherms confirm the presence of both physisorption and chemisorption. For TBBI, apart from the adsorption of the benzimidazole ring and sulfydryl group, the introduction of benzyl ring increases the electron density in the TBBI molecules. TBBI molecules could also adsorb on Fe surface by forming feedback bonds at the benzene ring. Therefore, a higher inhibition efficiency of TBBI is present in both weight loss and electrochemical measurements. In the case of BTBBI, besides the adsorptions of benzimidazole ring, sulfydryl group, and benzene ring, the introduced alkyl chain arranges far from the Fe surface to form a hydrophobic layer, which further improves the inhibition performance of BTBBI. Therefore, the inhibition efficiency of BTBBI is higher than those of MBI and TBBI. Both weight loss and electrochemical measurements, quantum chemical calculations and molecular dynamics (MD) simulations, indicate that the inhibition efficiencies of three benzimidazole derivatives follow the order: BTBBI > TBBI > MBI.

4. Conclusions

1. The inhibition performances of three kinds of benzimidazole derivatives (MBI,

TBBI, BTBBI) for the corrosion of mild steel in 1 M HCl solution were studied. Both the weight loss and electrochemical measurements indicate that these three inhibitors exhibit good inhibition performances and their efficiencies increase with the increasing concentration in the order: BTBBI > TBBI > MBI. The introduction of benzyl and alkyl chain to 2-mercaptobenzimidazole (MBI) prominently improves the inhibition performance.

2. These three benzimidazole derivatives act as mixed type inhibitors with predominant cathodic effectiveness. Their adsorptions follow the Langmuir adsorption isotherm. The adsorption of MBI and TBBI includes physisorption and chemisorption while adsorption of BTBBI is typical chemisorption.
3. Quantum chemical calculations reveal the order of the inhibition efficiencies of these three benzimidazole derivatives: BTBBI > TBBI > MBI, which is in accordance with the experimental results.
4. Molecular dynamics simulation indicates that the three benzimidazole derivatives adsorb on Fe (1 1 0) surface in flat orientation. For BTBBI, the alkyl chain arranges far from the Fe surface to form a hydrophobic layer, which further improves the inhibition efficiency of BTBBI.

Acknowledgements

The authors thank the support of National Natural Science Foundation of China (Nos. 51571097, 51371086). The authors also thank the support of analytical and testing center of Huazhong University of Science and Technology.

References

[1] M. Finsgar, J. Jackson, Application of corrosion inhibitors for steels in acidic media for the oil and gas industry: A review, Corros Sci, 86 (2014) 17-41.

[2] A.A. Farag, T.A. Ali, The enhancing of 2-pyrazinecarboxamide inhibition effect on the acid corrosion of carbon steel in presence of iodide ions, J Ind Eng Chem, 21 (2015) 627-634.

[3] P. Dohare, K.R. Ansari, M.A. Quraishi, I.B. Obot, Pyranpyrazole derivatives as novel corrosion inhibitors for mild steel useful for industrial pickling process: Experimental and Quantum Chemical study, J Ind Eng Chem, 52 (2017) 197-210.

[4] A. Popova, E. Sokolova, S. Raicheva, M. Christov, AC and DC study of the temperature effect on mild steel corrosion in acid media in the presence of benzimidazole derivatives, Corros Sci, 45 (2003) 33-58.

[5] A. Popova, M. Christov, S. Raicheva, E. Sokolova, Adsorption and inhibitive properties of benzimidazole derivatives in acid mild steel corrosion, Corros Sci, 46 (2004) 1333-1350.

[6] I. Ahamad, M.A. Quraishi, Bis (benzimidazol-2-yl) disulphide: An efficient water soluble inhibitor for corrosion of mild steel in acid media, Corros Sci, 51 (2009) 2006-2013.

[7] M. Prabakaran, S.H. Kim, N. Mugila, V. Hemapriya, K. Parameswari, S. Chitra, I.M. Chung, Aster koraiensis as nontoxic corrosion inhibitor for mild steel in sulfuric acid, J Ind Eng Chem, 52 (2017) 235-242.

[8] P.B. Matad, P.B. Mokshanatha, N. Hebbar, V.T. Venkatesha, H.C. Tandon, Ketosulfone Drug as a Green Corrosion Inhibitor for Mild Steel in Acidic Medium, Ind Eng Chem Res, 53 (2014) 8436-8444.

[9] H. Lgaz, R. Salghi, S. Jodeh, B. Hammouti, Effect of clozapine on inhibition of mild steel corrosion in 1.0 M HCl medium, J Mol Liq, 225 (2017) 271-280.

[10] M. Srivastava, P. Tiwari, S.K. Srivastava, R. Prakash, G. Ji, Electrochemical investigation of Irbesartan drug molecules as an inhibitor of mild steel corrosion in 1 M HCl and 0.5 M H2SO4 solutions, J Mol Liq, 236 (2017) 184-197.

[11] V. Srivastava, J. Haque, C. Verma, P. Singh, H. Lgaz, R. Salghi, M.A. Quraishi, Amino acid based imidazolium zwitterions as novel and green corrosion inhibitors for mild steel: Experimental, DFT and MD studies, J Mol Liq, 244 (2017) 340-352.

[12] W.H. Li, Q. He, C.L. Pei, B.R. Hou, Experimental and theoretical investigation of the adsorption behaviour of new triazole derivatives as inhibitors for mild steel corrosion in acid media, Electrochim Acta, 52 (2007) 6386-6394.

[13] M. Bouklah, B. Hammouti, M. Lagrenee, F. Bentiss, Thermodynamic properties of 2,5-bis(4-methoxyphenyl)-1,3,4-oxadiazole as a corrosion inhibitor for mild steel in normal sulfuric acid medium, Corros Sci, 48 (2006) 2831-2842.

[14] X.M. Wang, H.Y. Yang, F.H. Wang, An investigation of benzimidazole derivative as corrosion inhibitor for mild steel in different concentration HCl solutions, Corros Sci, 53 (2011) 113-121.

[15] N.A. Negm, N.G. Kandile, E.A. Badr, M.A. Mohammed, Gravimetric and electrochemical evaluation of environmentally friendly nonionic corrosion inhibitors for carbon steel in 1 M HCl, Corros Sci, 65 (2012) 94-103.

[16] J. Aljourani, M.A. Golozar, K. Raeissi, The inhibition of carbon steel corrosion in hydrochloric and sulfuric acid media using some benzimidazole derivatives, Mater Chem Phys, 121 (2010) 320-325.

[17] B.D. Mert, A.O. Yuce, G. Kardas, B. Yazici, Inhibition effect of 2-amino-4-methylpyridine on mild steel corrosion: Experimental and theoretical investigation, Corros Sci, 85 (2014) 287-295.

[18] R. Yildiz, A. Doner, T. Dogan, I. Dehri, Experimental studies of 2-pyridinecarbonitrile as corrosion inhibitor for mild steel in hydrochloric acid solution, Corros Sci, 82 (2014) 125-132.

[19] J. Haque, K.R. Ansari, V. Srivastava, M.A. Quraishi, I.B. Obot, Pyrimidine derivatives as novel acidizing corrosion inhibitors for CrossMark N80 steel useful for petroleum industry: A combined experimental and theoretical approach, J Ind Eng Chem, 49 (2017) 176-188.

[20] M. Bozorg, T.S. Farahani, J. Neshati, Z. Chaghazardi, G.M. Ziarani, Myrtus Communis as Green Inhibitor of Copper Corrosion in Sulfuric Acid, Ind Eng Chem Res, 53 (2014) 4295-4303.

[21] J. Aljourani, K. Raeissi, M.A. Golozar, Benzimidazole and its derivatives as corrosion inhibitors for mild steel in 1M HCl solution, Corros Sci, 51 (2009) 1836-1843.

[22] Y.M. Tang, F. Zhang, S.X. Hu, Z.Y. Cao, Z.L. Wu, W.H. Jing, Novel benzimidazole derivatives as corrosion inhibitors of mild steel in the acidic media. Part I: Gravimetric, electrochemical, SEM and XPS studies, Corros Sci, 74 (2013) 271-282.

[23] Y. Abboud, A. Abourriche, T. Saffaj, M. Berrada, M. Charrouf, A. Bennamara, A. Cherqaoui, D. Takky, The inhibition of mild steel corrosion in acidic medium by 2,2 '-bis(benzimidazole), Appl Surf Sci, 252 (2006) 8178-8184.

[24] F. Zhang, Y.M. Tang, Z.Y. Cao, W.H. Jing, Z.L. Wu, Y.Z. Chen, Performance and theoretical study on corrosion inhibition of 2-(4-pyridyl)-benzimidazole for mild steel in hydrochloric acid, Corros Sci, 61 (2012) 1-9.

[25] I.B. Obot, U.M. Edouk, Benzimidazole: Small planar molecule with diverse anti-corrosion potentials, J Mol Liq, 246 (2017) 66-90.

[26] A. Dutta, S.K. Saha, U. Adhikari, P. Banerjee, D. Sukul, Effect of substitution on corrosion inhibition properties of 2-(substituted phenyl) benzimidazole derivatives on mild steel in 1 M HCl solution: A combined experimental and theoretical approach, Corros Sci, 123 (2017) 256-266.

[27] A. Dutta, S.K. Saha, P. Banerjee, D. Sukul, Correlating electronic structure with corrosion inhibition potentiality of some bis-benzimidazole derivatives for mild steel in hydrochloric acid: Combined experimental and theoretical studies, Corros Sci, 98 (2015) 541-550.

[28] E. Gutierrez, J.A. Rodriguez, J. Cruz-Borbolla, J.G. Alvarado-Rodriguez, P. Thangarasu, Development of a predictive model for corrosion inhibition of carbon steel by imidazole and benzimidazole derivatives, Corros Sci, 108 (2016) 23-35.

[29] K.F. Khaled, The inhibition of benzimidazole derivatives on corrosion of iron in 1 M HCl solutions, Electrochim Acta, 48 (2003) 2493-2503.

[30] J. Cruz, R. Martinez, J. Genesca, E. Garcia-Ochoa, Experimental and theoretical study of 1-(2-ethylamino)-2-methylimidazoline as an inhibitor of carbon steel corrosion in acid media, J Electroanal Chem, 566 (2004) 111-121.

[31] B. Xu, W.N. Gong, K.G. Zhang, W.Z. Yang, Y. Liu, X.S. Yin, H. Shi, Y.Z. Chen, Theoretical prediction and experimental study of 1-Butyl-2-(4-methylphenyl)benzimidazole as a novel corrosion inhibitor for mild steel in hydrochloric acid, J Taiwan Inst Chem E, 51 (2015) 193-200.

[32] M. Yadav, S. Kumar, T. Purkait, L.O. Olasunkanmi, I. Bahadur, E.E. Ebenso, Electrochemical, thermodynamic and quantum chemical studies of synthesized benzimidazole derivatives as corrosion inhibitors for N80 steel in hydrochloric acid, J Mol Liq, 213 (2016) 122-138.

[33] D.Q. Zhang, Y.M. Tang, S.J. Qi, D.W. Dong, H. Cang, G. Lu, The inhibition performance of long-chain alkyl-substituted benzimidazole derivatives for corrosion of mild steel in HCl, Corros Sci, 102 (2016) 517-522.

[34] J. Zhang, J.X. Liu, W.Z. Yu, Y.G. Yan, L. You, L.F. Liu, Molecular modeling of the inhibition mechanism of 1-(2-aminoethyl)-2-alkyl-imidazoline, Corros Sci, 52 (2010) 2059-2065.

[35] O. Benali, L. Larabi, M. Traisnel, L. Gengembre, Y. Harek, Electrochemical, theoretical and XPS studies of 2-mercapto-1-methylimidazole adsorption on carbon steel in 1 M HClO4, Appl Surf Sci, 253 (2007) 6130-6139.

[36] F. Bentiss, M. Lebrini, M. Lagrenee, Thermodynamic characterization of metal dissolution and inhibitor adsorption processes in mild steel/2,5-bis(n-thienyl)-1,3,4-thiadiazoles/hydrochloric acid system, Corros Sci, 47 (2005) 2915-2931.

[37] R.V. Kumar, K.R. Gopal, K.V.S.R.S. Kumar, Facile synthesis and antimicrobial properties of 2-(Substituted-benzylsulfanyl)-1H-benzimidazoles, J Heterocyclic Chem, 42 (2005) 1405-1408.

[38] V.V. Torres, V.A. Rayol, M. Magalhaes, G.M. Viana, L.C.S. Aguiar, S.P. Machado, H. Orofino, E. D'Elia, Study of thioureas derivatives synthesized from a green route as corrosion inhibitors for mild steel in HCl solution, Corros Sci, 79 (2014) 108-118.

[39] H.H. Hassan, E. Abdelghani, M.A. Amin, Inhibition of mild steel corrosion in hydrochloric acid solution by triazole derivatives - Part I. Polarization and EIS studies, Electrochim Acta, 52 (2007) 6359-6366.

[40] Y.J. Qiang, S.T. Zhang, L. Guo, X.W. Zheng, B. Xiang, S.J. Chen, Experimental and theoretical studies of four allyl imidazolium-based ionic liquids as green inhibitors for copper corrosion in sulfuric acid, Corros Sci, 119 (2017) 68-78.

[41] F.G. Liu, M. Du, J. Zhang, M. Qiu, Electrochemical behavior of Q235 steel in saltwater saturated with carbon dioxide based on new imidazoline derivative inhibitor, Corros Sci, 51 (2009) 102-109.

[42] A.Y. Musa, R.T.T. Jalgham, A. Mohamad, Molecular dynamic and quantum chemical calculations for phthalazine derivatives as corrosion inhibitors of mild steel in 1 M HCl, Corros Sci, 56 (2012) 176-183.

[43] M. Behpour, S.M. Ghoreishi, N. Soltani, M. Salavati-Niasari, M. Hamadanian, A. Gandomi, Electrochemical and theoretical investigation on the corrosion inhibition of mild steel by thiosalicylaldehyde derivatives in hydrochloric acid solution, Corros Sci, 50 (2008) 2172-2181.

[44] M.A. Hegazy, H.M. Ahmed, A.S. El-Tabei, Investigation of the inhibitive effect of p-substituted 4-(N,N,N-dimethyldodecylammonium bromide)benzylidene-benzene-2-yl-amine on corrosion of carbon steel pipelines in acidic medium, Corros Sci, 53 (2011) 671-678.

[45] X.W. Zheng, S.T. Zhang, W.P. Li, L.L. Yin, J.H. He, J.F. Wu, Investigation of 1-butyl-3-methyl-1H-benzimidazolium iodide as inhibitor for mild steel in sulfuric acid solution,

Corros Sci, 80 (2014) 383-392.

[46] K.R. Ansari, M.A. Quraishi, A. Singh, Schiff's base of pyridyl substituted triazoles as new and effective corrosion inhibitors for mild steel in hydrochloric acid solution, Corros Sci, 79 (2014) 5-15.

[47] X.H. Li, S.D. Deng, H. Fu, Triazolyl blue tetrazolium bromide as a novel corrosion inhibitor for steel in HCl and H2SO4 solutions, Corros Sci, 53 (2011) 302-309.

[48] A. Kosari, M.H. Moayed, A. Davoodi, R. Parvizi, M. Momeni, H. Eshghi, H. Moradi, Electrochemical and quantum chemical assessment of two organic compounds from pyridine derivatives as corrosion inhibitors for mild steel in HCl solution under stagnant condition and hydrodynamic flow, Corros Sci, 78 (2014) 138-150.

[49] S.A. Ali, H.A. Al-Muallem, S.U. Rahman, M.T. Saeed, Bis-isoxazolidines: A new class of corrosion inhibitors of mild steel in acidic media, Corros Sci, 50 (2008) 3070-3077.

[50] L. Guo, S.H. Zhu, S.T. Zhang, Experimental and theoretical studies of benzalkonium chloride as an inhibitor for carbon steel corrosion in sulfuric acid, J Ind Eng Chem, 24 (2015) 174-180.

[51] N.D. Gowraraju, S. Jagadeesan, K. Ayyasamy, L.O. Olasunkanmi, E.E. Ebenso, C. Subramanian, Adsorption characteristics of Iota-carrageenan and Inulin biopolymers as potential corrosion inhibitors at mild steel/sulphuric acid interface, J Mol Liq, 232 (2017) 9-19.

[52] B.C. Tan, S.T. Zhang, Y.J. Qiang, L. Feng, C.H. Liao, Y. Xu, S.J. Chen, Investigation of the inhibition effect of Montelukast Sodium on the copper corrosion in 0.5 mol/L H2SO4, J Mol Liq, 248 (2017) 902-910.

[53] D.M. Gurudatt, K.N. Mohana, Synthesis of New Pyridine Based 1,3,4-Oxadiazole Derivatives and their Corrosion Inhibition Performance on Mild Steel in 0.5 M Hydrochloric Acid, Ind Eng Chem Res, 53 (2014) 2092-2105.

[54] M. Muralisankar, R. Sreedharan, S. Sujith, N.S.P. Bhuvanesh, A. Sreekanth, N(1)-pentyl isatin-N(4)-methyl-N(4)-phenyl thiosemicarbazone (PITSc) as a corrosion inhibitor on mild steel in HCl, J Alloy Compd, 695 (2017) 171-182.

[55] G. Gece, The use of quantum chemical methods in corrosion inhibitor studies, Corros Sci, 50 (2008) 2981-2992.

[56] D. Daoud, T. Douadi, H. Hamani, S. Chafaa, M. Al-Noaimi, Corrosion inhibition of mild steel by two new S-heterocyclic compounds in 1 M HCl: Experimental and computational study, Corros Sci, 94 (2015) 21-37.

[57] Z. El Adnani, M. Mcharfi, M. Sfaira, M. Benzakour, A.T. Benjelloun, M.E. Touhami, DFT theoretical study of 7-R-3methylquinoxalin-2(1H)-thiones (R=H; CH3; Cl) as corrosion inhibitors in hydrochloric acid, Corros Sci, 68 (2013) 223-230.

[58] N. Kovacevic, A. Kokalj, Analysis of molecular electronic structure of imidazole- and benzimidazole-based inhibitors: A simple recipe for qualitative estimation of chemical hardness, Corros Sci, 53 (2011) 909-921.

[59] S.D. Deng, X.H. Li, X.G. Xie, Hydroxymethyl urea and 1,3-bis(hydroxymethyl) urea as corrosion inhibitors for steel in HCl solution, Corros Sci, 80 (2014) 276-289.

[60] B. Xu, W.Z. Yang, Y. Liu, X.S. Yin, W.N. Gong, Y.Z. Chen, Experimental and theoretical evaluation of two pyridinecarboxaldehyde thiosemicarbazone compounds as corrosion inhibitors for mild steel in hydrochloric acid solution, Corros Sci, 78 (2014) 260-268.

Table 1 Fitted electrochemical parameters of the EIS of mild steel in 1 M HCl solution without or with various concentrations of benzimdazole derivative inhibitors at 30 ^{o}C for 1 h

Inhibitor	Concentration (mg/L)	R_s (Ω cm^2)	C_{dl} (μF/cm^2)	R_{ct} (Ω cm^2)	η_{EIS} (%)	θ
Without inhibitor	0	0.74	172.2	9.33	-	-
MBI	10	0.52	148.4	19.49	55.6	0.556
	25	0.62	84.2	51.72	82.0	0.820
	50	0.71	43.3	119.78	92.2	0.922
	75	0.73	36.4	152.10	93.9	0.939
	100	0.71	32.1	187.90	95.0	0.950
TBBI	10	1.16	84.0	21.1	55.8	0.558
	25	0.78	69.2	61.6	84.9	0.849
	50	0.91	33.4	177.1	94.7	0.947
	75	1.07	21.1	257.5	96.4	0.964
	100	1.16	18.5	362.9	97.4	0.974
BTBBI	10	0.65	23.9	414.8	97.7	0.977
	25	0.53	19.2	550.6	98.3	0.983
	50	0.69	18.3	655.8	98.6	0.986
	75	0.46	17.8	807.8	98.8	0.988
	100	0.47	17.2	1052.1	99.1	0.991

Table 2 Fitted electrochemical parameters of the EIS of mild steel in 1 M HCl solution without or with different concentrations of BTBBI inhibitor at different temperatures for 1 h

Temperature (^{o}C)	Concentration (mg/L)	R_s (Ω cm^2)	C_{dl} (μF/cm^2)	R_{ct} (Ω cm^2)	η_{EIS} (%)	θ
40	0	1.11	343.2	4.63	-	-
	10	0.94	93.5	109.6	95.8	0.958
	25	0.99	61.1	169.3	97.2	0.972
	50	1.02	47.7	237.2	98.1	0.981
	75	0.96	51.9	250.1	98.2	0.982
	100	0.98	46.7	288.3	98.4	0.984
50	0	1.03	376	3.89		
	10	0.98	95.4	78.6	95.1	0.951
	25	1.05	45.8	110.6	96.4	0.964
	50	0.91	43.4	147.4	97.4	0.974
	75	0.97	36.5	193.4	98.0	0.980
	100	0.83	41.1	252.7	98.4	0.984
60	0	0.97	497	1.98		
	10	0.93	150	36.4	94.6	0.946
	25	1.04	46.8	58.0	96.6	0.966
	50	0.84	42.8	79.4	97.5	0.975
	75	0.89	37.1	85.9	97.7	0.977
	100	0.99	41.2	122.2	98.3	0.983

Table 3 Fitted electrochemical parameters of the polarization curves of mild steel in 1 M HCl solution without or with various concentrations of benzimdazole derivative inhibitors at 30 ^{o}C for 1 h

Inhibitor	Concentration (mg/L)	E_{corr} (V vs.SCE)	i_{corr} (A/cm^2)	b_a (mV/dec)	b_c (mV/dec)	η_p (%)
Without inhibitor	0	-0.483	2.37×10^{-3}	165	-130	-
MBI	10	-0.496	4.24×10^{-4}	161	-85	82.1
	25	-0.501	3.02×10^{-4}	170	-93	87.3
	50	-0.512	1.52×10^{-4}	166	-114	93.6
	75	-0.509	1.23×10^{-4}	159	-115	94.8
	100	-0.501	7.95×10^{-5}	146	-110	96.6
TBBI	10	-0.535	3.47×10^{-4}	95	-85	85.4
	25	-0.493	1.87×10^{-4}	76	-114	92.1
	50	-0.508	4.94×10^{-5}	80	-109	97.9
	75	-0.527	4.30×10^{-5}	92	-116	98.2
	100	-0.519	4.03×10^{-5}	87	-120	98.3
BTBBI	10	-0.519	4.57×10^{-5}	68	-126	98.3
	25	-0.524	4.08×10^{-5}	65	-137	98.5
	50	-0.503	2.12×10^{-5}	71	-135	99.2
	75	-0.522	2.02×10^{-5}	73	-140	99.3
	100	-0.512	1.50×10^{-5}	74	-140	99.4

Table 4 Fitted electrochemical parameters of the potentiodynamic polarization curves of mild steel in 1 M HCl solution without or with different concentrations of BTBBI inhibitor at different temperatures for 1 h

Temperature (^{o}C)	Concentration (mg/L)	E_{corr} (V vs.SCE)	i_{corr} (A/cm^2)	b_a (mV/dec)	b_c (mV/dec)	η_p (%)
40	Without inhibitor	-0.499	0.0088	199	-184	
	10	-0.509	0.000218	101	-160	97.5
	25	-0.515	0.000165	122	-160	98.1
	50	-0.518	0.000148	68	-174	98.3
	75	-0.519	6.01×10^{-5}	187	-162	99.3
	100	-0.521	5.26×10^{-5}	119	-175	99.4
50	Without inhibitor	-0.496	0.0096	168	-195	
	10	-0.513	0.000238	86	-105	97.5
	25	-0.506	0.000188	93	-124	98.0
	50	-0.508	0.000164	61	-128	98.3
	75	-0.507	7.61×10^{-5}	64	-133	99.2
	100	-0.516	6.60×10^{-5}	82	-121	99.3
60	Without inhibitor	-0.495	0.0132	186	-196	
	10	-0.506	0.000736	64	-140	94.7
	25	-0.517	0.000284	107	-129	97.9
	50	-0.511	0.000229	71	-138	98.3
	75	-0.519	0.000167	74	-127	98.8
	100	-0.511	0.000101	79	-142	99.2

Table 5 Standard thermodynamic and equilibrium adsorption parameters for the adsorption of three benzimdazole derivative inhibitors on mild steel surface in 1 M HCl solution at 30 ^{o}C

Inhibitor	Slope	Intercept (mmol/L)	Linear correlation coefficient	K_{ads} (L/mol)	ΔG^{o}_{ads} (kJ/mol)
MBI	0.98	0.04548	0.998	21987.7	-35.32
TBBI	0.97	0.02797	0.998	35752.6	-36.55
BTBBI	1.01	0.000797	0.999	1254705	-45.52

Table 6 Thermodynamic parameters for the adsorption of BTBBI inhibitor on mild steel surface in 1 M HCl solution at different temperatures

Temperature (^{o}C)	K_{ads} (L/mol)	ΔG^{o}_{ads} (kJ/mol)	ΔH^{o}_{ads} (kJ/mol)	ΔS^{o}_{ads} (J/(mol K))
30	1254705	-45.52	-38.41	23.46
40	729927	-45.58		22.92
50	465116	-45.83		22.97
60	318471	-46.20		23.39

Table 7 Thermodynamic parameters for the adsorption of BTBBI inhibitors on mild steel surface in 1 M HCl solution at different temperatures

Inhibitors	E_a (kJ/mol)	ΔH^{o}_{a} (kJ/mol)	ΔS^{o}_{a} (J/(mol k))
Without inhibitor	51.73	49.09	-131.76
MBI	56.20	53.56	-141.96
TBBI	54.12	51.48	-154.48
BTBBI	27.27	24.66	-246.41

Table 8 Quantum chemical parameters derived for benzimidazole derivative inhibitors calculated by DFT/GGA/BLYP method with DNP basis set

Molecule	E_{HOMO} (eV)	E_{LUMO} (eV)	ΔE (eV)	χ (eV)	γ (eV)	ΔN
MBI	-5.343	-1.493	3.850	3.418	1.925	0.930
TBBI	-5.197	-1.566	3.631	3.382	1.815	0.997
BTBBI	-5.180	-1.569	3.611	3.375	1.805	1.004

Table 9 Fukui indices of the three benzimdazole derivatives (MBI, TBBI, BTBBI)

Molecule	Atom	f_k^+	f_k^-	Molecule	Atom	f_k^+	f_k^-	Molecule	Atom	f_k^+	f_k^-
MBI	C1	0.066	0.077	TBBI	C1	0.020	0.064	BTBBI	C1	0.017	0.065
	C2	0.126	0.038		C2	0.035	0.032		C2	0.030	0.031
	C3	0.024	0.067		C3	0.010	0.060		C3	0.009	0.062
	C4	0.034	0.054		C4	0.008	0.050		C4	0.008	0.050
	C5	0.130	0.052		C5	0.036	0.044		C5	0.032	0.044
	C6	0.032	0.043		C6	0.011	0.041		C6	0.010	0.042
	N7	0.064	0.082		N7	0.023	0.072		N7	0.022	0.070
	C8	0.083	0.043		C8	0.029	0.035		C8	0.027	0.039
	N9	0.032	0.026		N9	0.004	0.030		N9	0	0.011
	S10	0.121	0.263		S10	0.125	0.275		S10	0.113	0.257
					C11	0.006	-0.020		C11	0.007	-0.017
					C12	0.045	-0.008		C12	0.050	-0.01
					C13	0.072	0.008		C13	0.039	0.007
					C14	0.020	0.005		C14	0.045	0.005
					C15	0.094	0.007		C15	0.099	0.007
					C16	0.045	0.006		C16	0.021	0.005
					C17	0.035	0.007		C17	0.073	0.007
									C18	-0.014	-0.014
									C19	-0.001	-0.003
									C20	0	-0.001
									C21	0	-0.001

Table 10 The adsorption energies between the three benzimdazole derivatives inhibitor molecules and Fe (1 1 0) surface

Inhibitors	E_{ads} (kJ/mol)
MBI	-341.77
TBBI	-569.15
BTBBI	-646.71

Highlights:

- Three kinds of benzimidazole derivatives were studied as inhibitors for mild steel.
- These inhibitors act as mixed type ones with predominant cathodic effectiveness.
- The adsorption of benzimidazole derivatives obey the Langmuir adsorption isotherm.
- Benzimidazole derivatives adsorb on Fe (1 1 0) surface with a flat orientation.

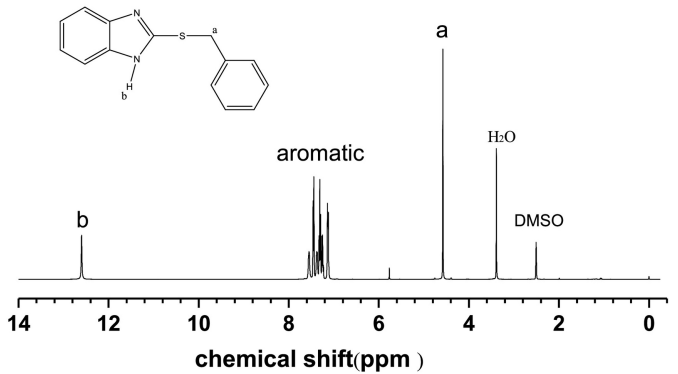
a
aromatic
H2O
DMSO
b
14
12
10
8
6
4
2
0
chemical shift(ppm)

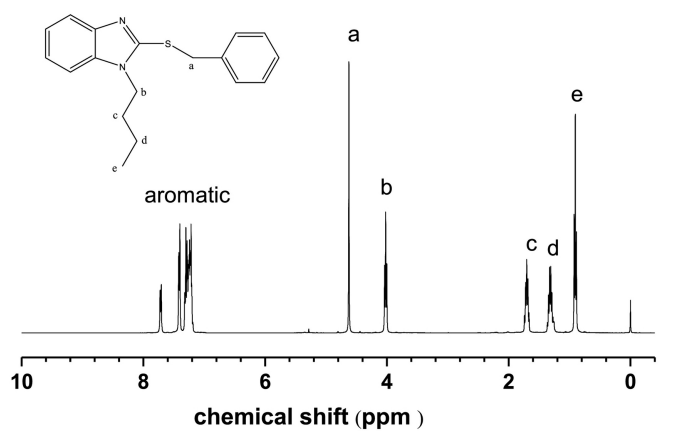
a
e
aromatic
b
c
d
10
8
6
4
2
0
chemical shift (ppm)

Figure 1

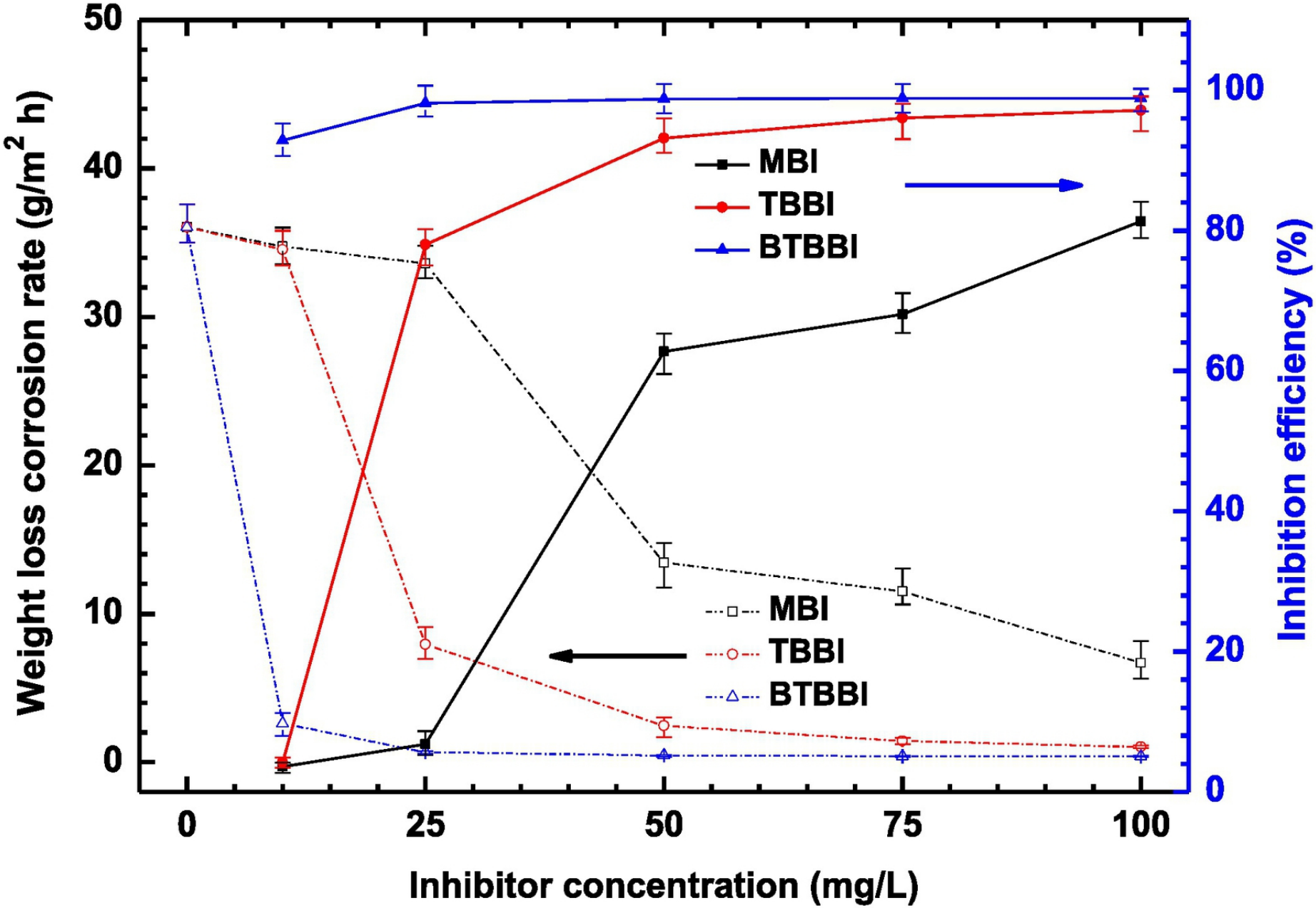
Weight loss corrosion rate (g/m^2 h)
Inhibition efficiency (%)
Inhibitor concentration (mg/L)
0
10
20
30
40
50
0
20
40
60
80
100
0
25
50
75
100
MBI
TBBI
BTBBI
MBI
TBBI
BTBBI

Figure 2

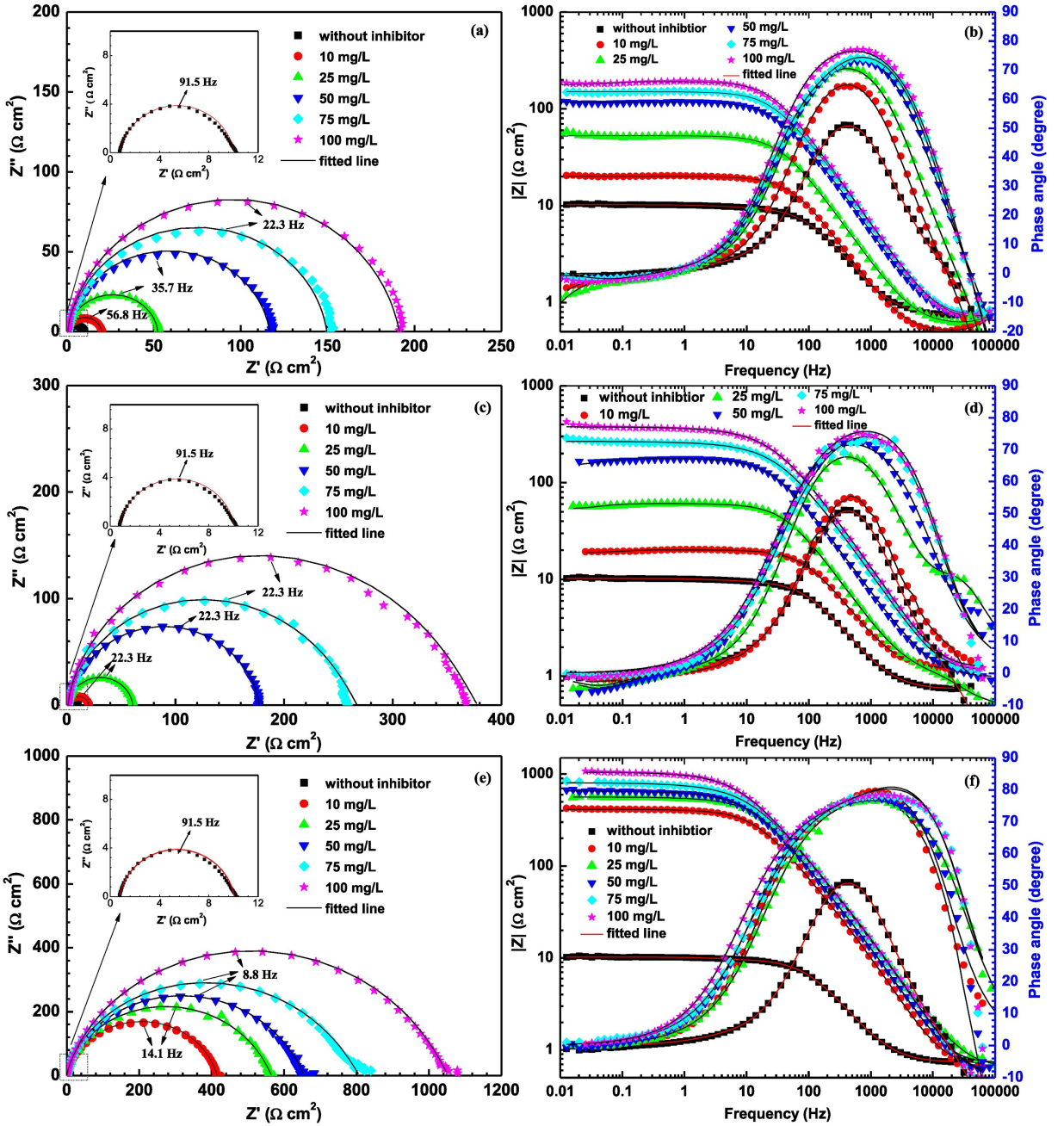
(a)
without inhibitor
10 mg/L
25 mg/L
50 mg/L
75 mg/L
100 mg/L
fitted line
91.5 Hz
22.3 Hz
35.7 Hz
56.8 Hz
Z'' (Ω cm²)
Z' (Ω cm²)
(b)
without inhibtior
10 mg/L
25 mg/L
50 mg/L
75 mg/L
100 mg/L
fitted line
|Z| (Ω cm²)
Phase angle (degree)
Frequency (Hz)
(c)
without inhibitor
10 mg/L
25 mg/L
50 mg/L
75 mg/L
100 mg/L
fitted line
91.5 Hz
22.3 Hz
22.3 Hz
22.3 Hz
Z'' (Ω cm²)
Z' (Ω cm²)
(d)
without inhibtior
10 mg/L
25 mg/L
50 mg/L
75 mg/L
100 mg/L
fitted line
|Z| (Ω cm²)
Phase angle (degree)
Frequency (Hz)
(e)
without inhibitor
10 mg/L
25 mg/L
50 mg/L
75 mg/L
100 mg/L
fitted line
91.5 Hz
8.8 Hz
14.1 Hz
Z'' (Ω cm²)
Z' (Ω cm²)
(f)
without inhibtior
10 mg/L
25 mg/L
50 mg/L
75 mg/L
100 mg/L
fitted line
|Z| (Ω cm²)
Phase angle (degree)
Frequency (Hz)

Figure 3

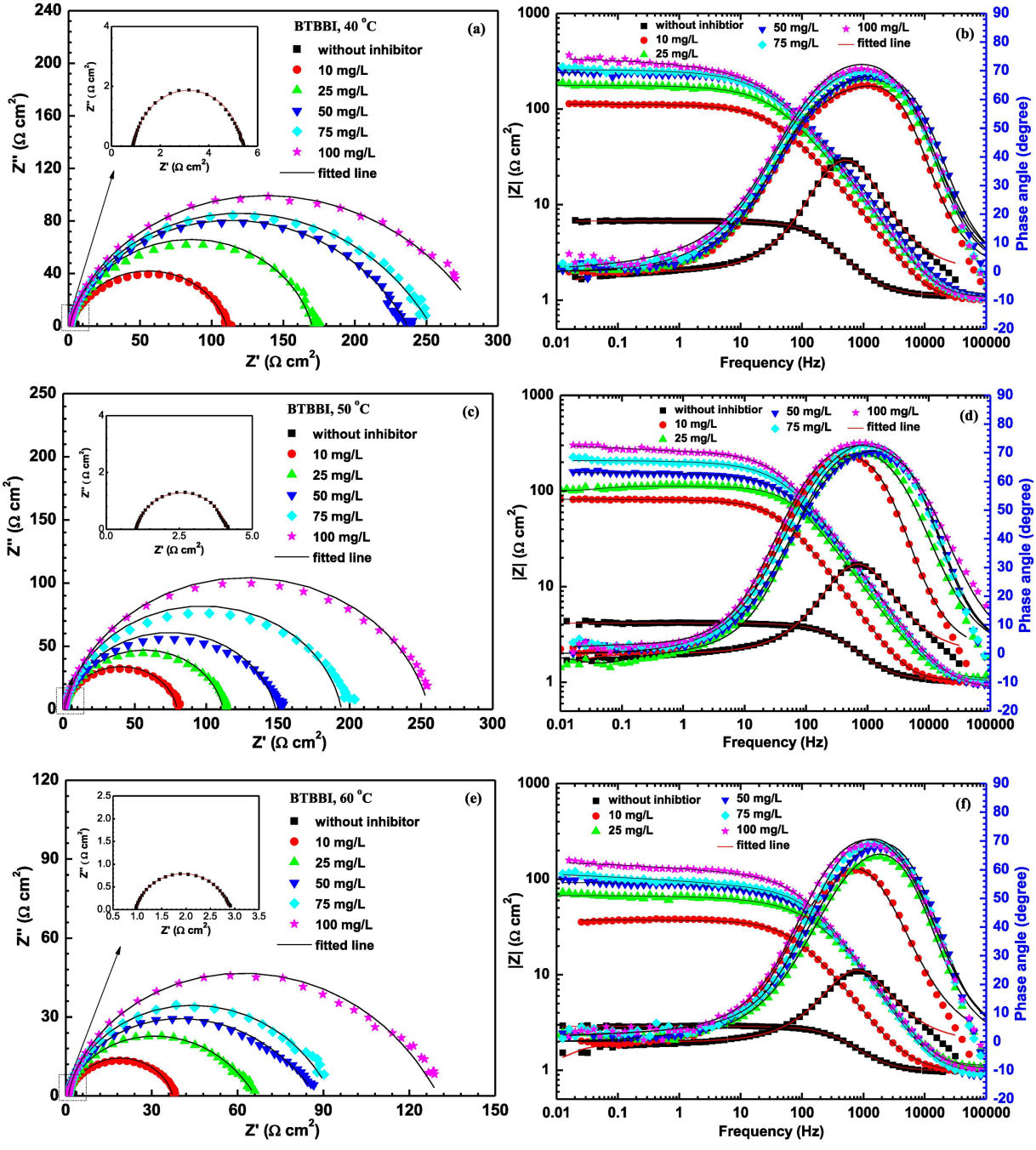
BTBBI, 40 °C
(a)
without inhibitor
10 mg/L
25 mg/L
50 mg/L
75 mg/L
100 mg/L
fitted line
Z'' (Ω cm²)
Z' (Ω cm²)
(b)
|Z| (Ω cm²)
Phase angle (degree)
Frequency (Hz)
BTBBI, 50 °C
(c)
(d)
BTBBI, 60 °C
(e)
(f)

Figure 4

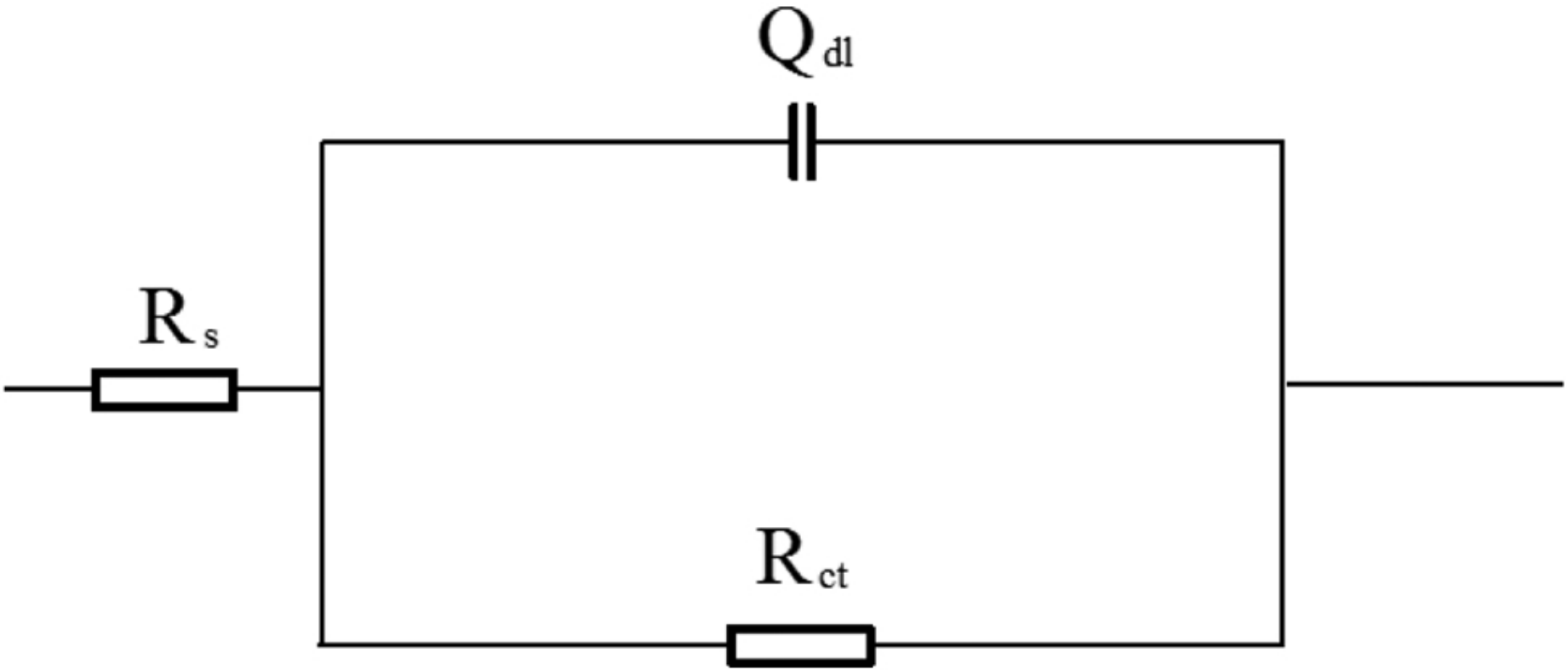

Figure 5

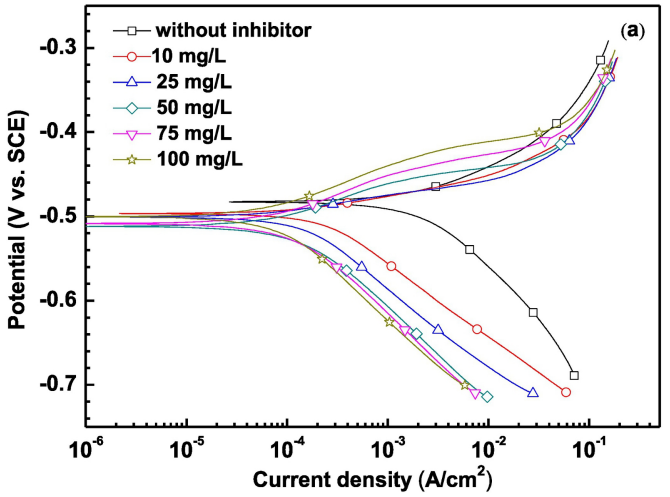
(a)
without inhibitor
10 mg/L
25 mg/L
50 mg/L
75 mg/L
100 mg/L
Potential (V vs. SCE)
-0.3
-0.4
-0.5
-0.6
-0.7
10-6
10-5
10-4
10-3
10-2
10-1
Current density (A/cm2)

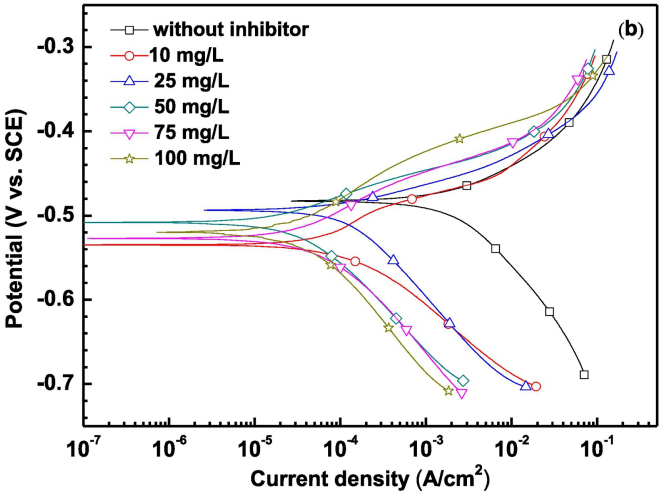
(b)
without inhibitor
10 mg/L
25 mg/L
50 mg/L
75 mg/L
100 mg/L
Potential (V vs. SCE)
-0.3
-0.4
-0.5
-0.6
-0.7
10-7
10-6
10-5
10-4
10-3
10-2
10-1
Current density (A/cm2)

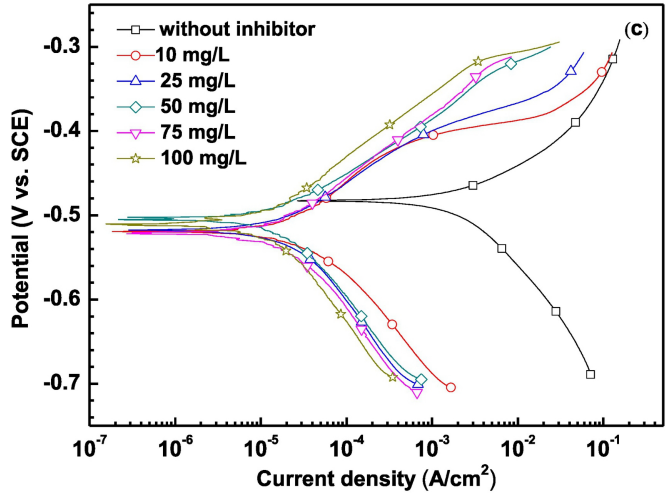
(c)
without inhibitor
10 mg/L
25 mg/L
50 mg/L
75 mg/L
100 mg/L
Potential (V vs. SCE)
-0.3
-0.4
-0.5
-0.6
-0.7
10-7
10-6
10-5
10-4
10-3
10-2
10-1
Current density (A/cm2)

Figure 6

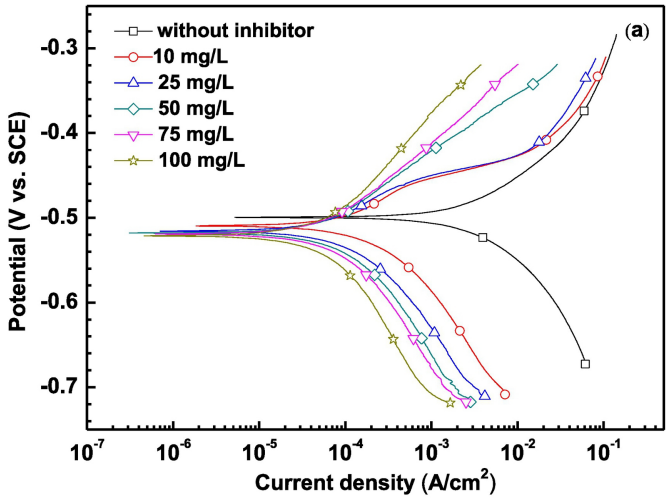
without inhibitor
10 mg/L
25 mg/L
50 mg/L
75 mg/L
100 mg/L
(a)
Potential (V vs. SCE)
-0.3
-0.4
-0.5
-0.6
-0.7
10^-7
10^-6
10^-5
10^-4
10^-3
10^-2
10^-1
Current density (A/cm^2)

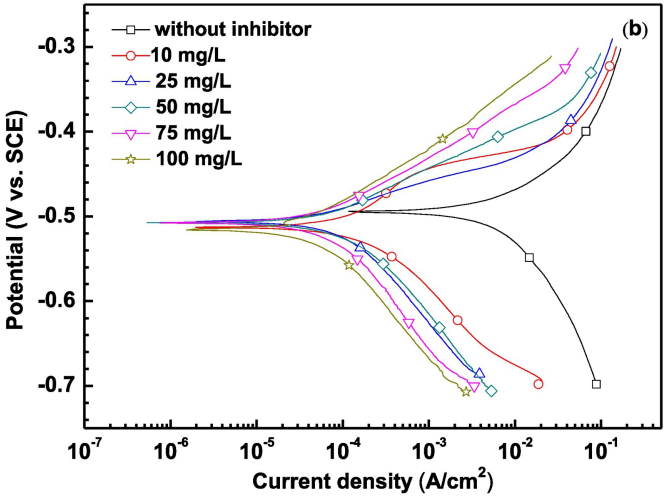
without inhibitor
10 mg/L
25 mg/L
50 mg/L
75 mg/L
100 mg/L
(b)
Potential (V vs. SCE)
-0.3
-0.4
-0.5
-0.6
-0.7
10^-7
10^-6
10^-5
10^-4
10^-3
10^-2
10^-1
Current density (A/cm^2)

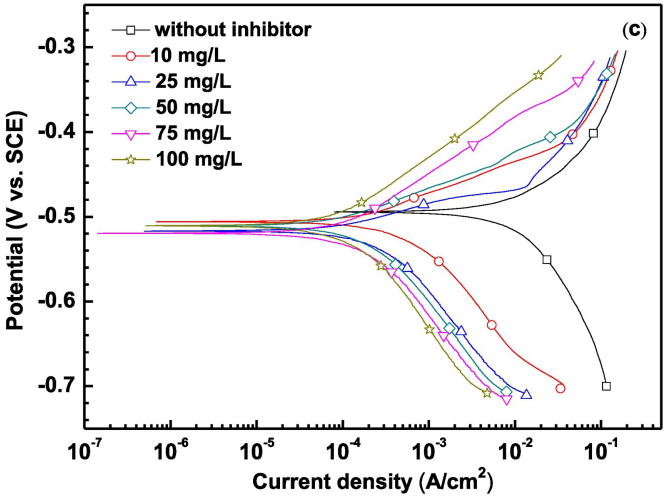
without inhibitor
10 mg/L
25 mg/L
50 mg/L
75 mg/L
100 mg/L
(c)
Potential (V vs. SCE)
-0.3
-0.4
-0.5
-0.6
-0.7
10^-7
10^-6
10^-5
10^-4
10^-3
10^-2
10^-1
Current density (A/cm^2)

Figure 7

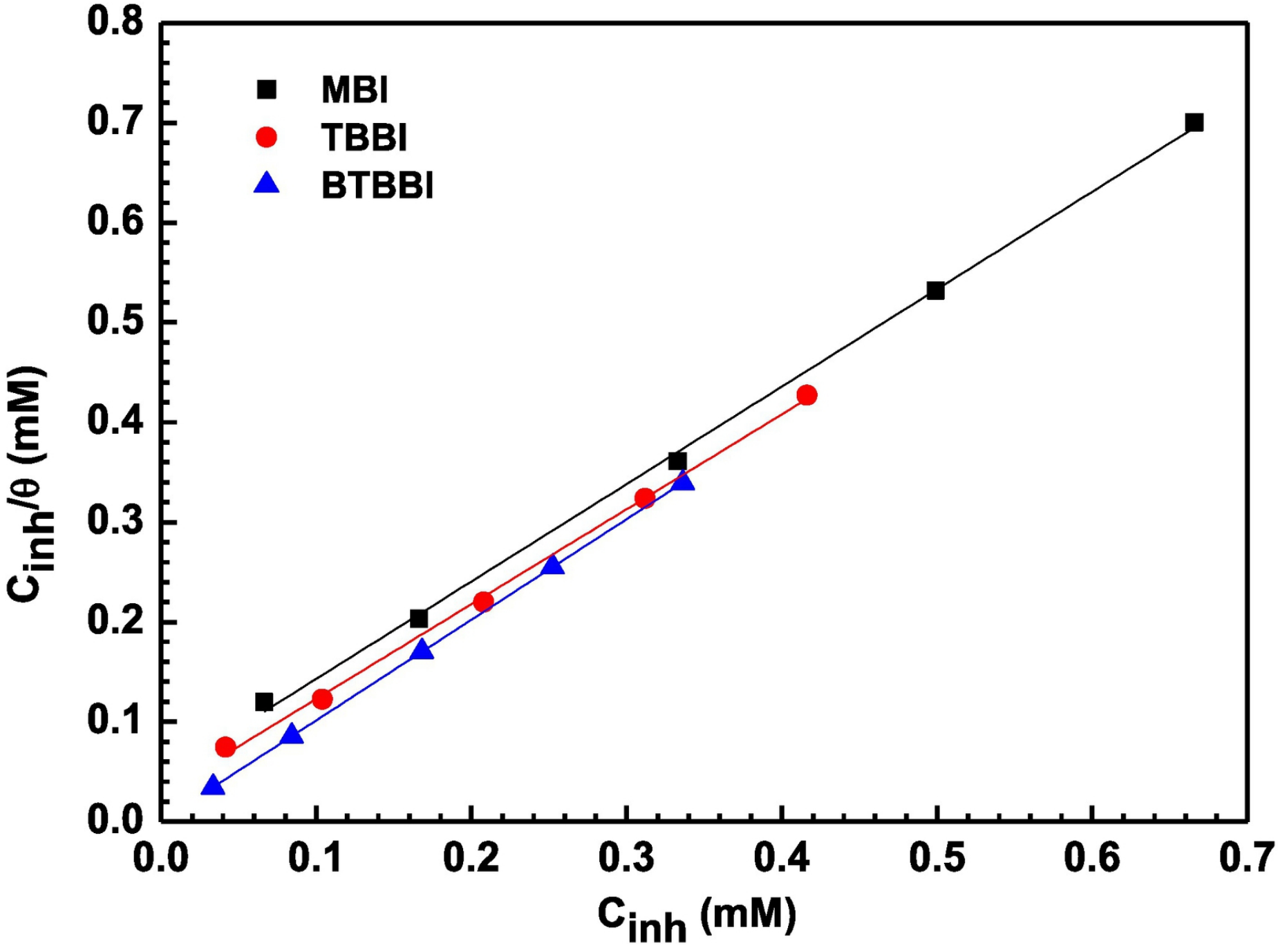

Figure 8

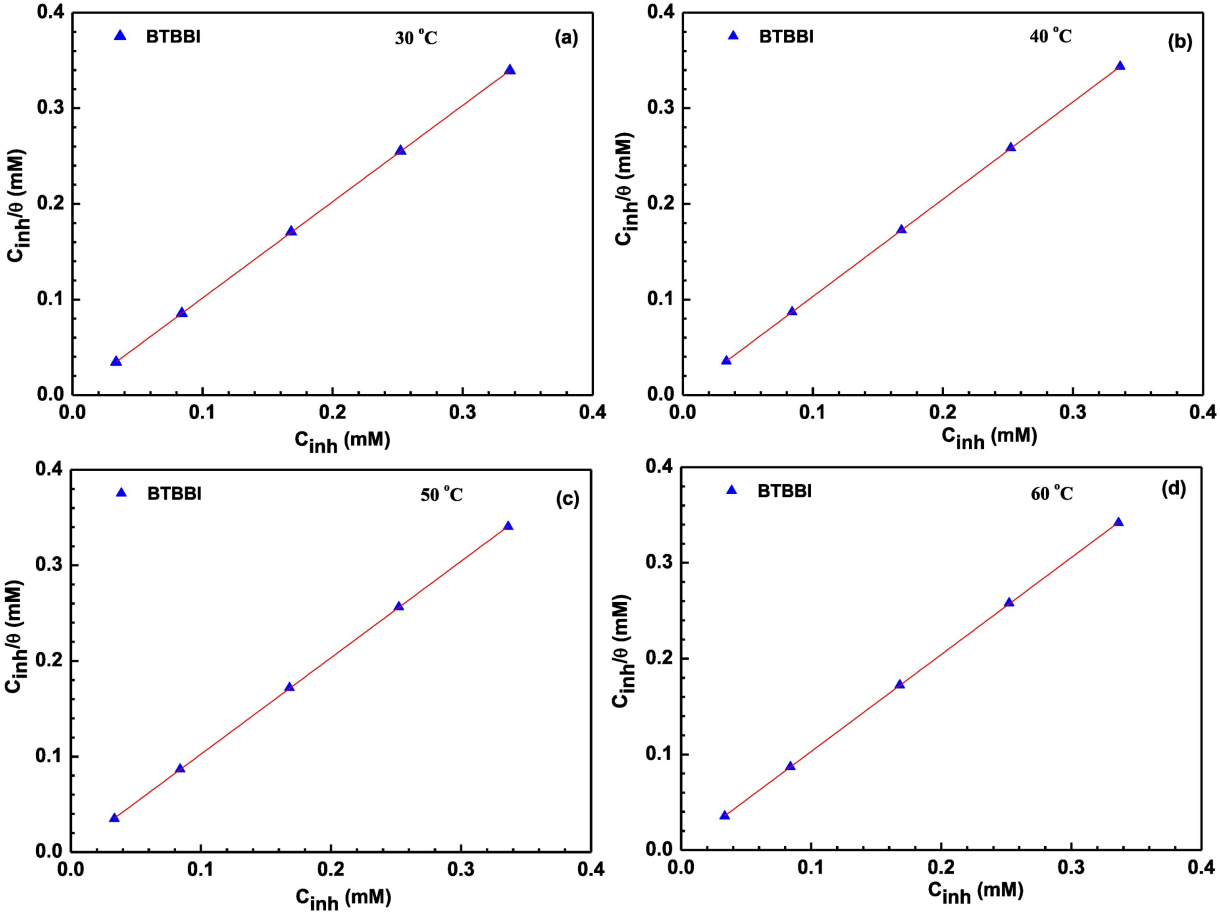
BTBBI
30 °C
(a)
BTBBI
40 °C
(b)
BTBBI
50 °C
(c)
BTBBI
60 °C
(d)
C_{inh}/θ (mM)
C_{inh} (mM)
0.0
0.1
0.2
0.3
0.4

Figure 9

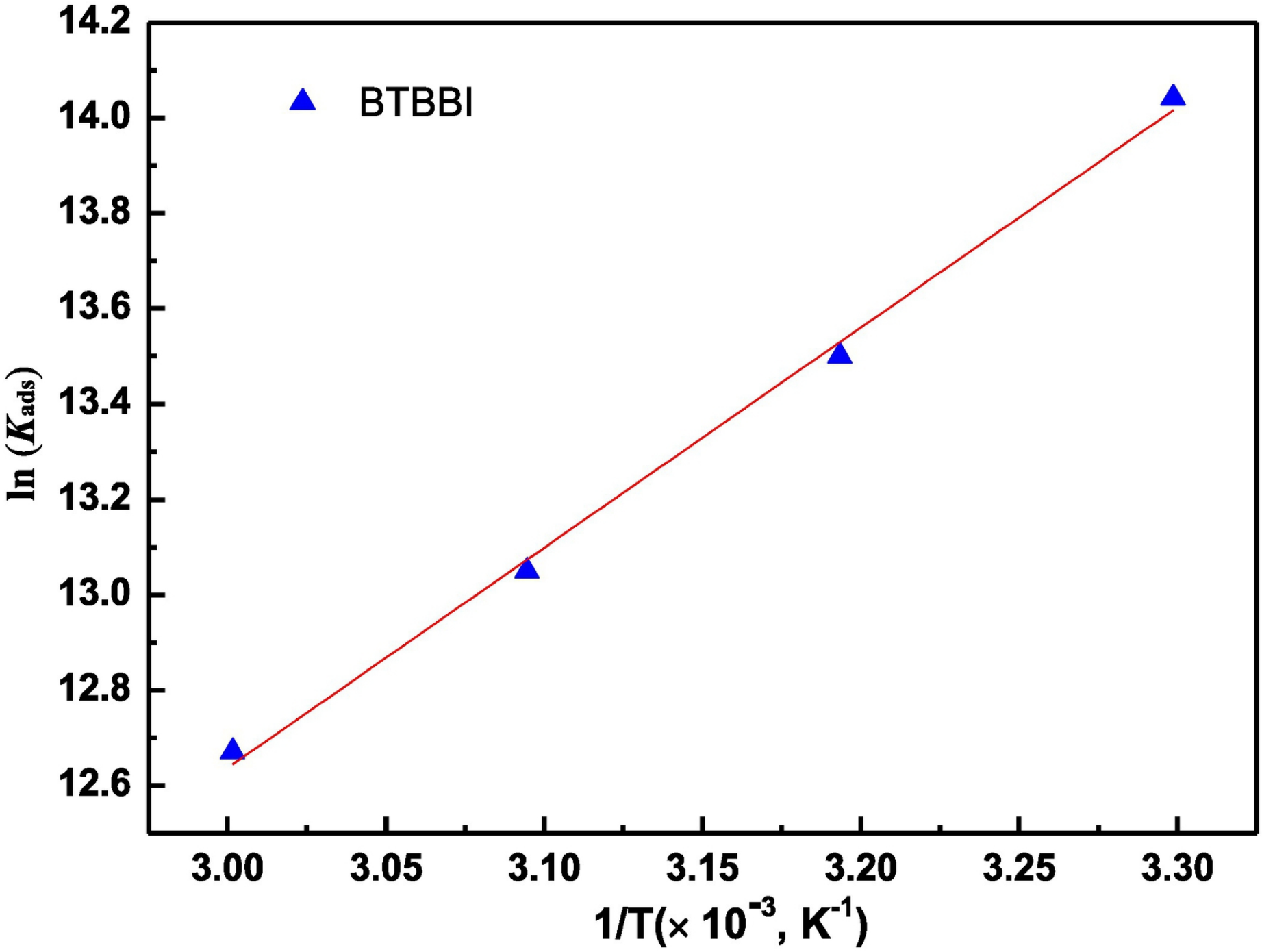
BTBBI
14.2
14.0
13.8
13.6
13.4
13.2
13.0
12.8
12.6
ln (K_{ads})
3.00
3.05
3.10
3.15
3.20
3.25
3.30
1/T(× 10^{-3}, K^{-1})

Figure 10

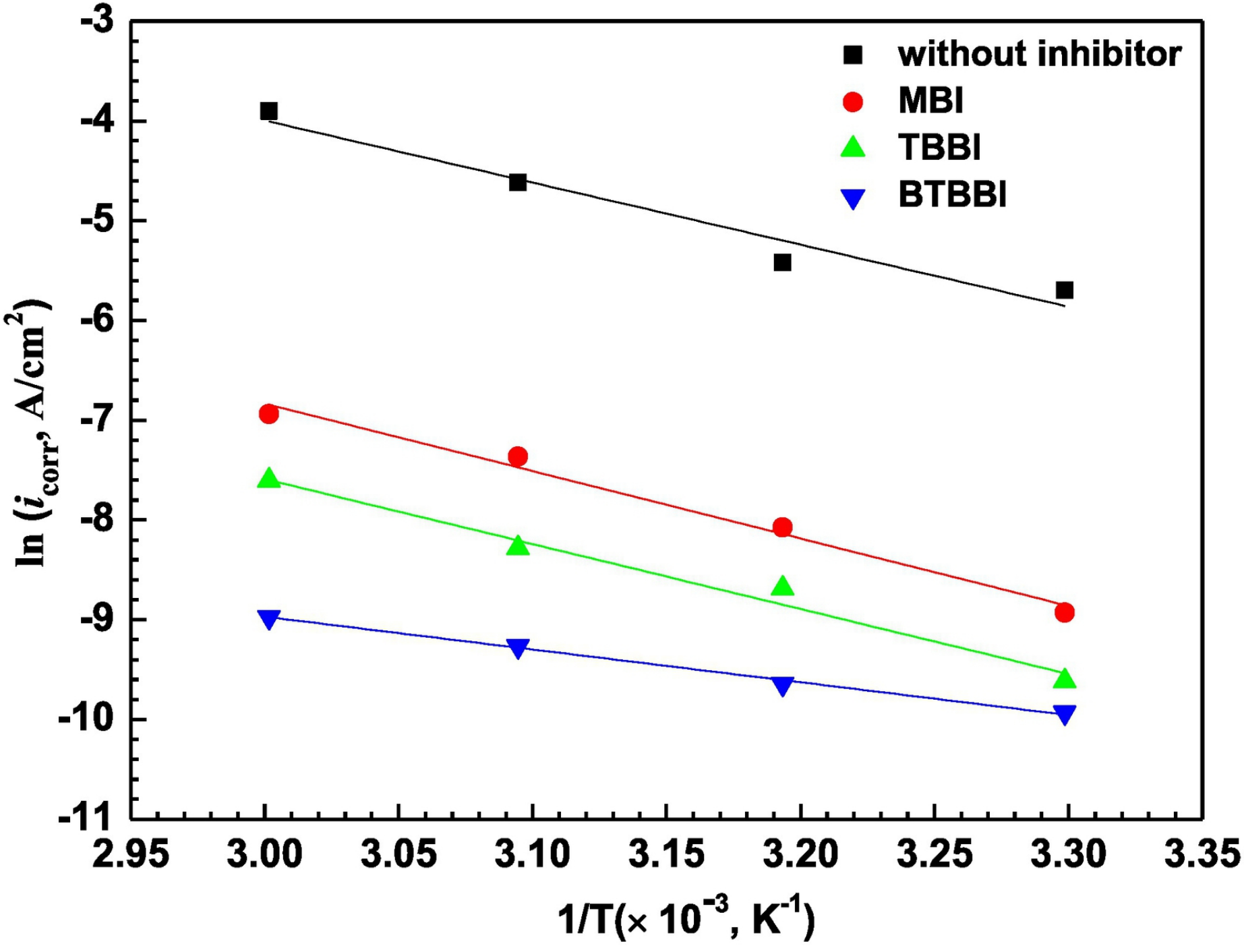
without inhibitor
MBI
TBBI
BTBBI
ln (i_{corr}, A/cm^2)
1/T(× 10^{-3}, K^{-1})
-3
-4
-5
-6
-7
-8
-9
-10
-11
2.95
3.00
3.05
3.10
3.15
3.20
3.25
3.30
3.35

Figure 11

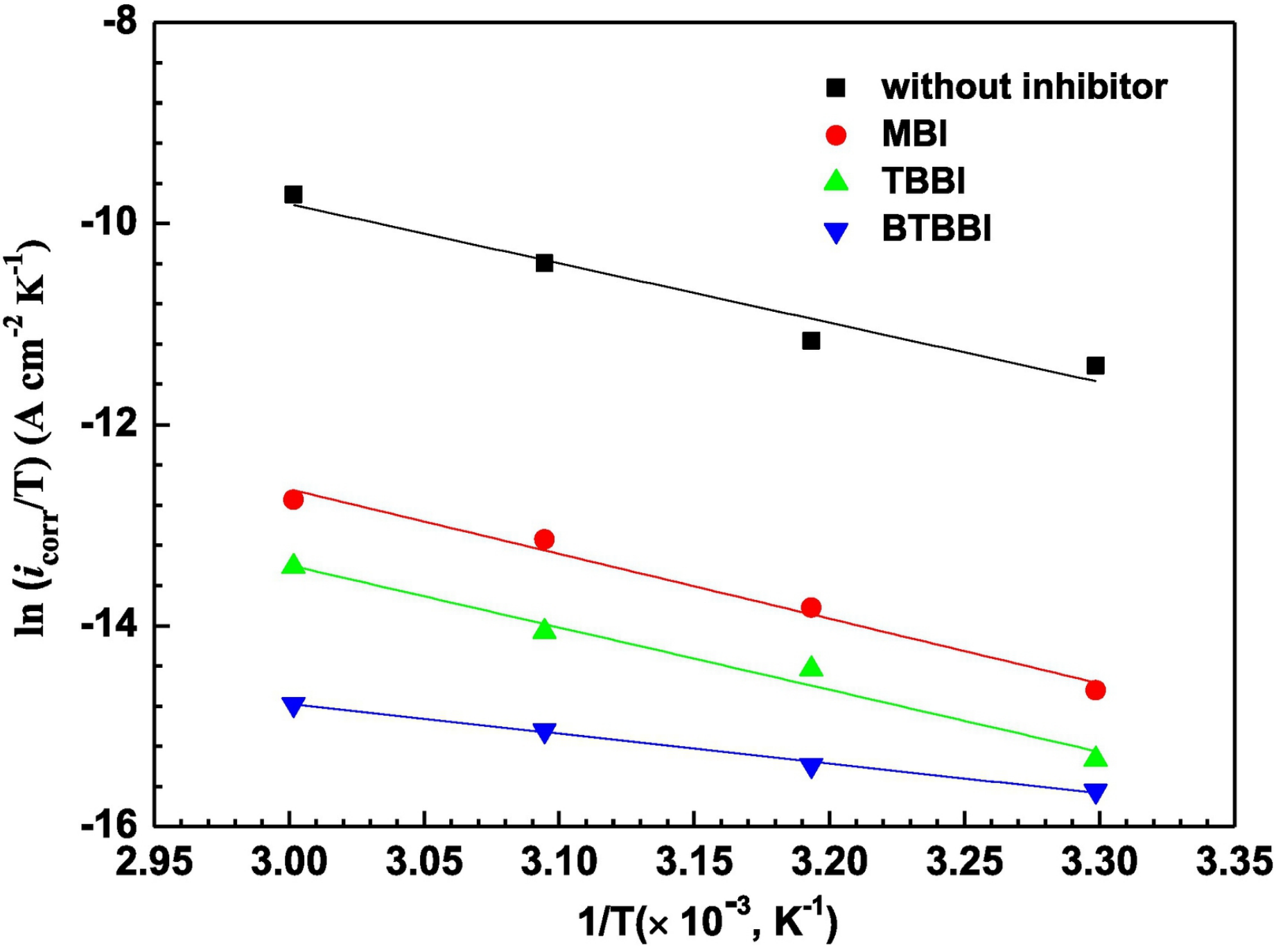
without inhibitor
MBI
TBBI
BTBBI
ln (i_{corr}/T) (A cm^{-2} K^{-1})
1/T(× 10^{-3}, K^{-1})
-8
-10
-12
-14
-16
2.95
3.00
3.05
3.10
3.15
3.20
3.25
3.30
3.35

Figure 12

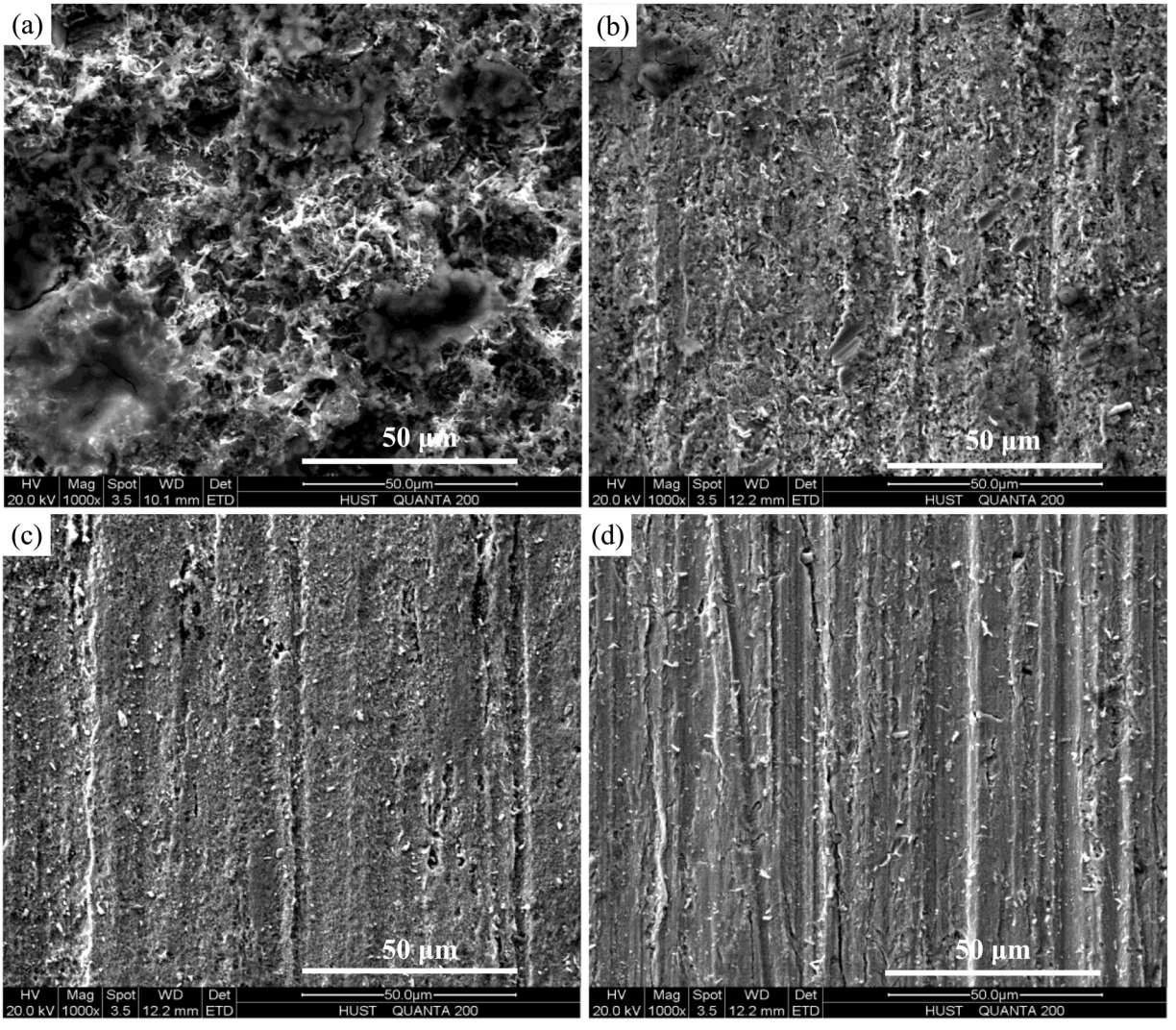
(a)
50 µm
HV 20.0 kV | Mag 1000x | Spot 3.5 | WD 10.1 mm | Det ETD
50.0µm
HUST QUANTA 200
(b)
50 µm
HV 20.0 kV | Mag 1000x | Spot 3.5 | WD 12.2 mm | Det ETD
50.0µm
HUST QUANTA 200
(c)
50 µm
HV 20.0 kV | Mag 1000x | Spot 3.5 | WD 12.2 mm | Det ETD
50.0µm
HUST QUANTA 200
(d)
50 µm
HV 20.0 kV | Mag 1000x | Spot 3.5 | WD 12.2 mm | Det ETD
50.0µm
HUST QUANTA 200

Figure 13

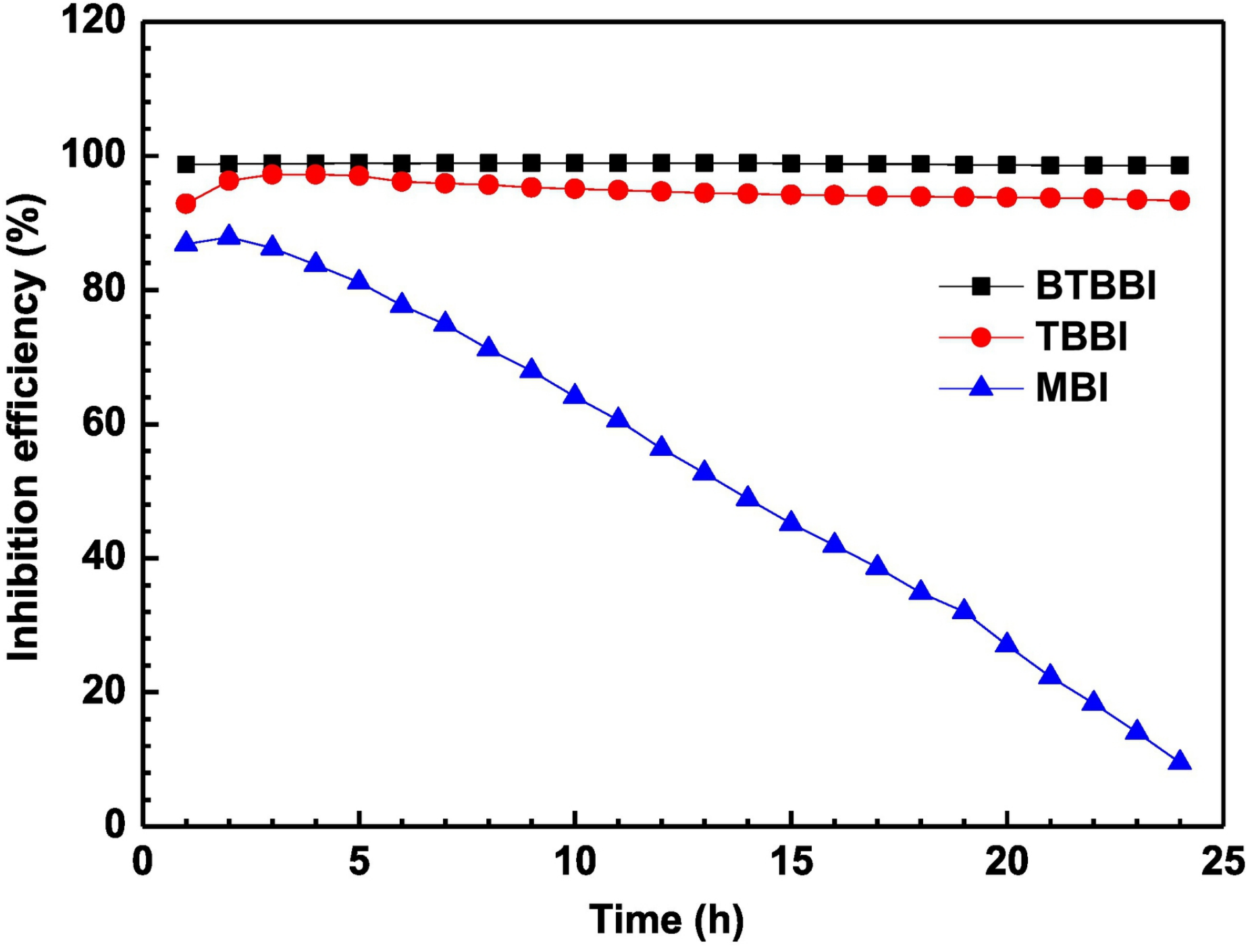
120
100
80
60
40
20
0
Inhibition efficiency (%)
0
5
10
15
20
25
Time (h)
BTBBI
TBBI
MBI

Figure 14

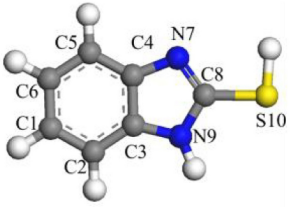

MBI

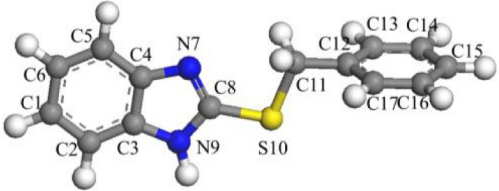

TBBI

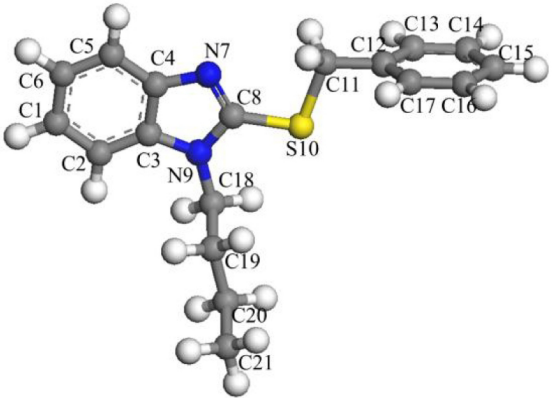

BTBBI

Figure 15

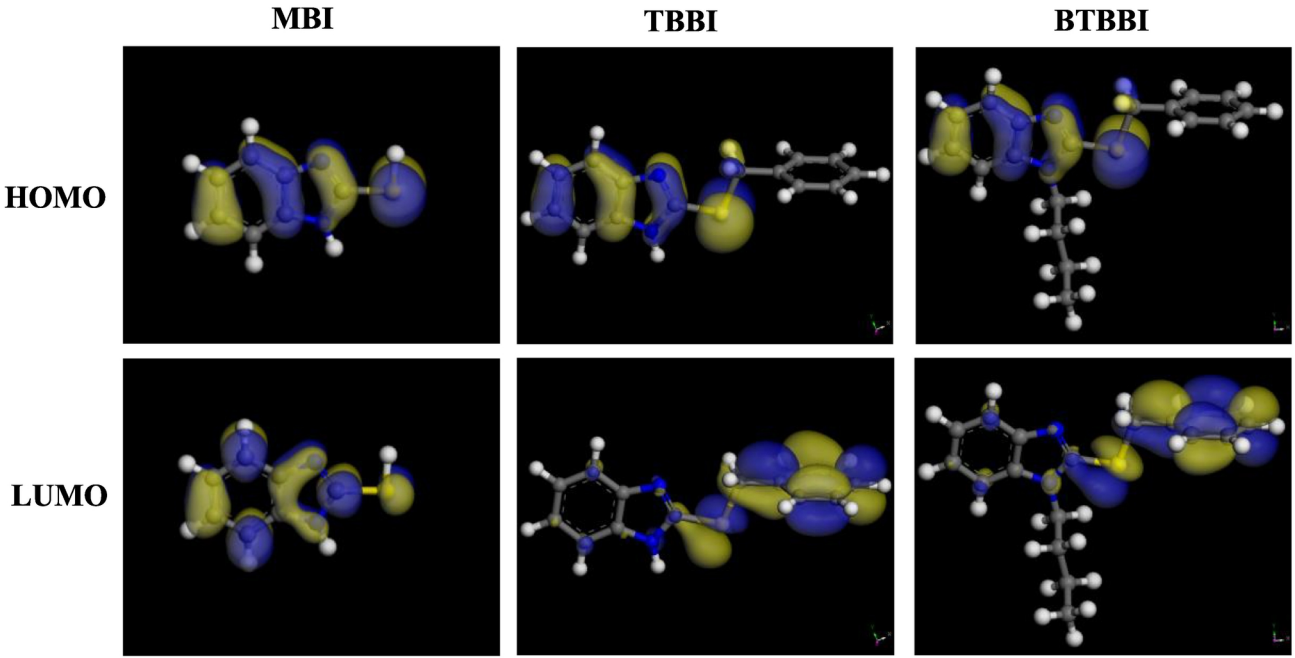

Figure 16

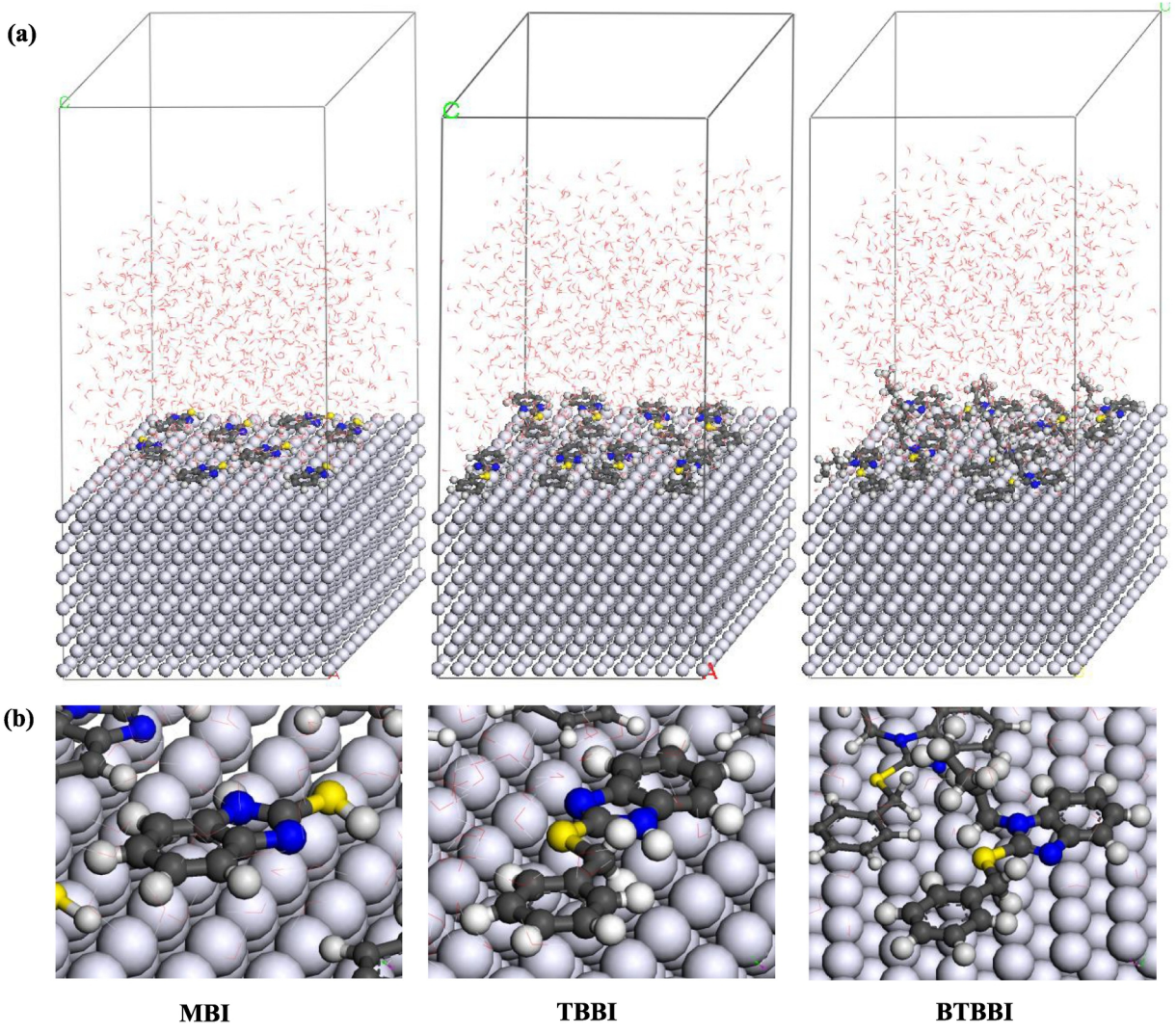

Figure 17

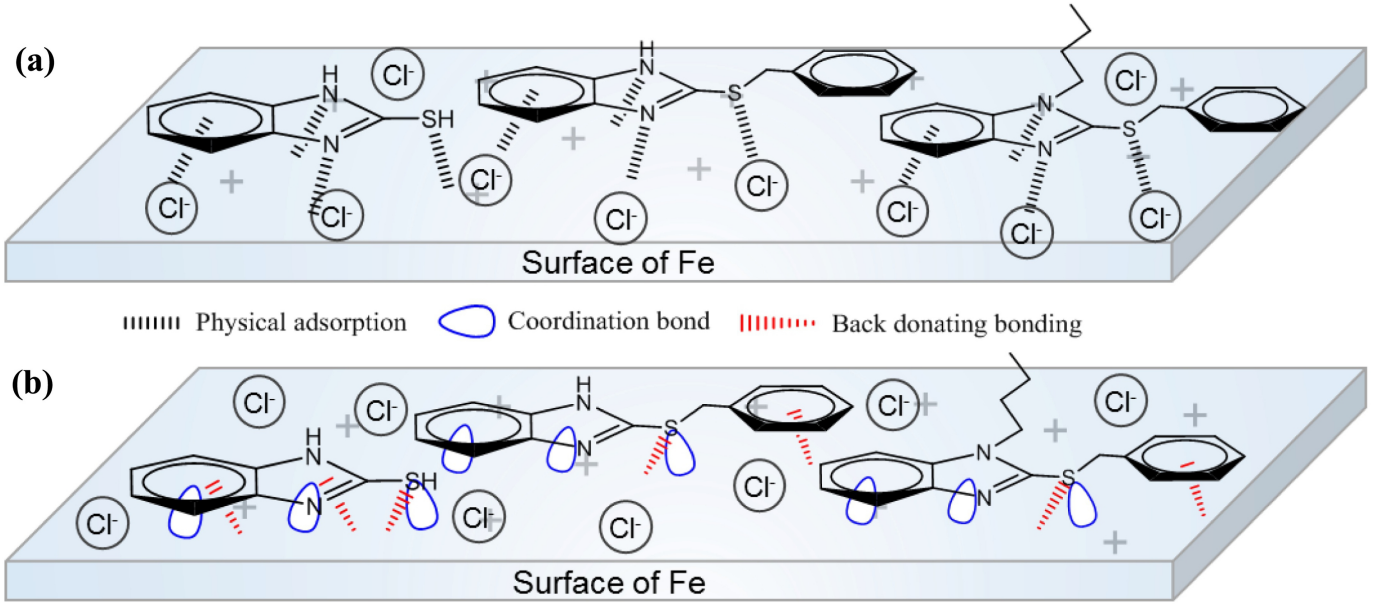
(a)
Cl-
SH
S
Surface of Fe
Physical adsorption
Coordination bond
Back donating bonding
(b)
Surface of Fe

Figure 18